HHS Public Access

Author manuscript

Cell Rep. Author manuscript; available in PMC 2023 December 18.

Published in final edited form as:

Cell Rep. 2023 August 29; 42(8): 112993. doi:10.1016/j.celrep.2023.112993.

Transplantation elicits a clonally diverse CD8+ T cell response that is comprised of potent CD43+ effectors

Gregory S. Cohen[1], **Melissa A. Kallarakal**[1], **Sahana Jayaraman**[1], **Francis I. Ibukun**[1], **Katherine P. Tong**[2], **Linda D. Orzolek**[3], **H. Benjamin Larman**[1], **Scott M. Krummey**[1,4,*]

[1]Department of Pathology, Johns Hopkins School of Medicine, Baltimore, MD 21205, USA

[2]Emory Transplant Center, Emory University School of Medicine, Atlanta, GA 30322, USA

[3]Department of Molecular Biology and Genetics, Johns Hopkins School of Medicine, Baltimore, MD 21205, USA

[4]Lead contact

SUMMARY

CD8$^+$ T cells mediate acute rejection of allografts, which threatens the long-term survival of transplanted organs. Using MHC class I tetramers, we find that allogeneic CD8$^+$ T cells are present at an elevated naive precursor frequency relative to other epitopes, only modestly increase in number after grafting, and maintain high T cell receptor diversity throughout the immune response. While antigen-specific effector CD8$^+$ T cells poorly express the canonical effector marker KLRG-1, expression of the activated glycoform of CD43 defines potent effectors after transplantation. Activated CD43$^+$ effector T cells maintain high expression of the coreceptor induced T cell costimulator (ICOS) in the presence of CTLA-4 immunoglobulin (Ig), and dual CTLA-4 Ig/anti-ICOS treatment prolongs graft survival. These data demonstrate that graft-specific CD8$^+$ T cells have a distinct response profile relative to anti-pathogen CD8$^+$ T cells and that CD43 and ICOS are critical surface receptors that define potent effector CD8$^+$ T cell populations that form after transplantation.

Graphical abstract

*Correspondence: skrumme1@jhmi.edu.

AUTHOR CONTRIBUTIONS

Conceptualization, S.M.K., H.B.L., G.S.C., and S.J.; methodology, S.M.K., G.S.C., H.B.L., and S.J.; formal analysis, S.M.K., G.S.C., S.J., and H.B.L.; investigation, S.M.K., G.S.C., M.A.K., S.J., F.I.I., K.P.T., and L.A.O.; writing, S.M.K., G.S.C., and S.J.; visualization, S.M.K. and G.S.C.; supervision, S.M.K. and H.B.L.

SUPPLEMENTAL INFORMATION

Supplemental information can be found online at https://doi.org/10.1016/j.celrep.2023.112993.

DECLARATION OF INTERESTS

The authors declare no competing interests.

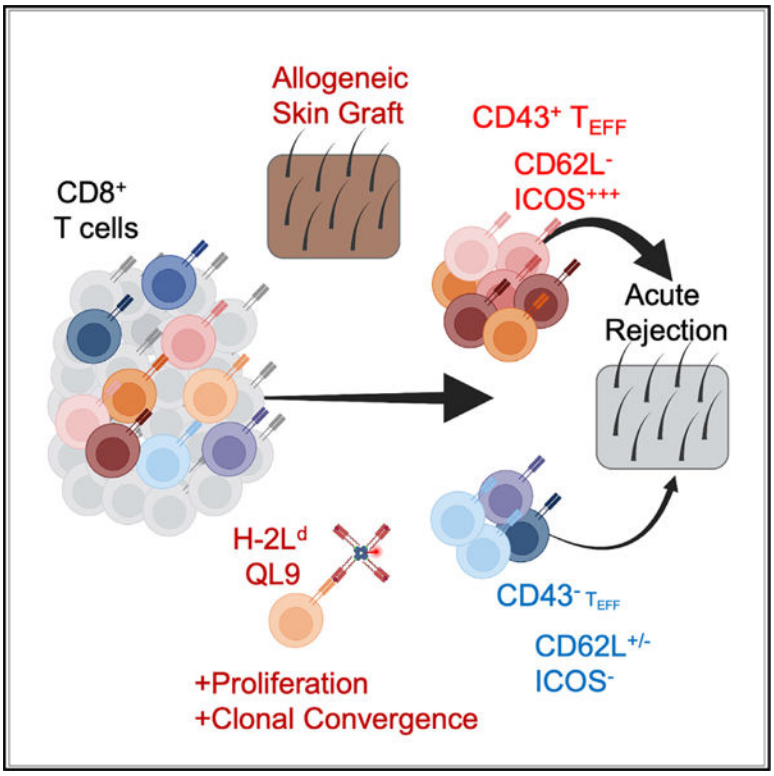

In brief

CD8$^+$ T cells mediate acute rejection, which is a barrier to long-term graft survival. Cohen et al. track endogenous graft-specific CD8$^+$ T cells during acute rejection of skin grafts and find that potent effector CD8$^+$ T cells are defined by the expression of the activated CD43 receptor.

INTRODUCTION

Activation of CD8$^+$ T cells relies on the recognition of cognate antigen in the presence of both coreceptor signaling and the local cytokine milieu.[1–3] The balance of these factors shapes the magnitude and character of the CD8$^+$ T cell response. In transplantation, CD8$^+$ T cells can respond to allogeneic antigen presented on donor major histocompatibility complex (MHC) class I proteins and can mediate tissue damage.[4,5] Recent clinical studies have highlighted that the occurrence of acute rejection has cumulative and detrimental effects on the long-term survival of transplanted organs.[6–8]

Activated T cells undergo several well-established phenotypic changes that distinguish them from quiescent naive CD8$^+$ T cells. The majority of the work underlying these paradigms has been performed in infection models, which present distinct profiles of inflammation and antigen relative to transplanted organs.[9–11] The canonical phenotype of an effector CD8$^+$ T cell, CD44^{hi}CD62L^{lo}, does not specifically distinguish the actively responding graft-specific CD8$^+$ T cells among the larger pool of previously activated cells. Expression of the surface receptor killer cell lectin-like receptor G1 (KLRG-1) is also used to identify actively responding effector CD8$^+$ T cells relative to memory precursor cells.[12–14] However,

KLRG-1 expression is not functionally required for the effector function of $CD8^+$ T cells, nor is it induced after all types of priming *in vivo.*[13,15] Thus, in order to more granularly understand anti-graft $CD8^+$ T cell responses and to develop strategies to target the allogeneic response, a deeper understanding of the differentiation program of post-graft $CD8^+$ T cells is needed.

Due to the technical difficulties associated with identifying allogeneic peptide epitopes, the $CD8^+$ T cell response is typically evaluated by using either T cell receptor (TCR) transgenic mice (e.g., OT-I/ovalbumin [OVA]) or by evaluating the "bulk" pool of activated $CD8^+$ T cells. Both approaches sacrifice potential insights gained by assessing the acutely responding antigen-specific T cell clones in the context of physiologic antigen levels, precursor frequency, clonal competition, and inflammatory signals. MHC tetramers have provided a tremendous advance in the ability to identify and track antigen-specific $CD8^+$ T cell responses to pathogens and model antigens.[16–19] However, the use of MHC tetramers to study allogeneic T cells has been limited due to the technical challenges of identifying appropriate epitopes from across the proteome.

We sought to develop the use of MHC tetramers in a fully allogeneic transplant model by taking advantage of elegant work performed in the characterization of the allogeneic 2C TCR transgenic mouse model several decades ago.[20–22] We found that MHC tetramers of an H-$2L^d$-restricted epitope for a ubiquitously expressed metabolic enzyme defined a population of $CD8^+$ T cells in H-2^b C57BL/6 mice. This approach allowed us to directly study the $CD8^+$ T cell response to fully allogeneic H-2^d grafts and to characterize the differentiation of effector populations in the context of physiologic antigen and inflammation. Here, we report the characteristics of the $CD8^+$ T cell response to allogeneic antigen, including the clonal features of antigen-specific alloreactive $CD8^+$ T cells, and of the emergence of a potent population of effector $CD8^+$ T cells that express the surface receptor CD43 after grafting.

RESULTS

MHC class I tetramer can be used to identify L^d $QL9^+$ $CD8^+$ T cells in naive C57BL/6 mice

Relatively few allogeneic epitopes have been identified in the fully allogeneic BALB/c (H-2^d) to C57BL/6 (H-2^b) transplant model. The alloreactive 2C TCR recognizes H-$2L^d$-restricted peptides for the self-peptide a-ketoglutarate dehydrogenase,[20–22] thus representing a directly presented allogeneic epitope. We hypothesized that MHC tetramers of this H-$2L^d$-restricted epitope could be used to identify endogenous alloreactive $CD8^+$ T cells. In order to reliably detect rare $CD8^+$ T cells, we incubated single-cell suspensions of secondary lymphoid organs with L^d QL9 tetramers and enriched for the tetramer fluorophore(s) using magnetic beads (Figure 1A).[23] This technique results in tetramer-enriched (column "bound") and bulk $CD8^+$ (column "unbound") fractions of cells for analysis.

In naive C57BL/6 mice, we detected a population of L^d QL9 tetramer-binding cells using phycoerythrin (PE) and allophycocyanin (APC) tetramers (Figure 1B). Using this approach, we identified L^d QL9-specific $CD8^+$ T cells in the spleen and lymph nodes (mean: 4,994 and 1,199 cells/tissue, respectively; Figures 1C and 1D). The number of C57BL/6 $CD8^+$ T

cells binding to the allogeneic L^d QL9 tetramer was significantly greater than the number of self-reactive L^d $QL9^+$ $CD8^+$ T cells found among BALB/c splenocytes (Figure 1C). Tetramer binding was specific, as no L^d QL9-binding cells were found in OT-I RAG1 knockout (KO) mice (Figure 1C). The phenotype of L^d QL9-binding $CD8^+$ T cells was largely $CD44^{lo}CD62L^{hi}$, similar to the phenotype of naive bulk $CD8^+$ T cells (Figure 1E). We found that the precursor frequency of K^b OVA and D^b LCMV gp33-specific $CD8^+$ T cells, while consistent with prior publications,[19] was significantly lower than that of L^d QL9 $CD8^+$ T cells (Figures 1F and 1G). Thus, the L^d QL9 tetramer specifically binds to a population of naive $CD8^+$ T cells that appear to be at a relatively elevated precursor frequency compared with other T cell populations.

L^d $QL9^+$ $CD8^+$ T cells become activated and proliferate in response to H-2^d BALB/c skin grafts

Having established that a population of H-2^b C57BL/6 $CD8^+$ T cells recognize L^d QL9 tetramers in naive mice, we next wanted to evaluate whether L^d $QL9^+$ $CD8^+$ T cells respond when presented with allogeneic H-$2L^d$ antigen-expressing tissue. In order to evaluate the magnitude and specificity of the L^d $QL9^+$ $CD8^+$ T cell response, we grafted skin from syngeneic H-2^b BALB/c, allogeneic H-2^d BALB/c, or third-party allogeneic H-2^k C3H mice onto C57BL/6 mice and assessed tetramer-binding $CD8^+$ T cells (Figures 2A and 2B). After C57BL/6 or C3H skin grafting, there was no significant increase in the number of $CD44^{hi}$ L^d $QL9^+$ $CD8^+$ T cells in the draining lymph nodes or spleen (Figures 2B and 2C). However, after BALB/c skin grafting, we found that a significant portion of L^d $QL9^+$ $CD8^+$ T cells became $CD44^{hi}$ on day 10 after skin grafting in the draining lymph nodes and spleen (Figure 2B). The absolute number of $CD44^{hi}$ L^d QL9 tetramer-binding cells increased by a mean of 10-fold in the draining lymph node and of 6.1-fold in the spleen versus naive C57BL/6 mice (Figure 2C).

T cells can recognize allogeneic antigen via direct, indirect, and semi-direct pathways.[24–27] As the contribution of the QL9 peptide bound to H-$2L^d$ during direct T cell allorecognition in our system is not clear, we evaluated the $CD8^+$ T cell response to additional H-$2L^d$ tetramers. We performed simultaneous tetramer staining with H-$2L^d$ tetramers containing QL9 peptide and either the closely related self-peptide LL9 or the unrelated murine leukemia virus (MuLV) $gp70_{423–431}$ peptide (Figure 2D). We evaluated the number of tetramer-binding $CD8^+$ T cells in C57BL/6 mice before and after BALB/c skin grafting. A significantly greater number of $CD8^+$ T cells bound to L^d QL9 tetramers than to L^d LL9 or L^d MuLV tetramers (Figure 2E). The number of L^d LL9- or L^d MuLV-binding $CD8^+$ T cells did not increase after BALB/c skin grafting (Figure 2E). Very few $CD8^+$ T cells simultaneously bound two tetramers, indicating that each tetramer-specific $CD8^+$ T cell population was distinct and that the $QL9^+$ $CD8^+$ T cell repertoire is not highly poly specific (Figure 2E). Overall, these data demonstrate that the QL9 peptide itself is a major determinant of the specificity of H-$2L^d$-specific C57BL/6 $CD8^+$ T cells.

In order to assess whether the phenotypic and cell number changes reflected a proliferative response in L^d QL9-specific $CD8^+$ T cells, we stained cells for Ki67 in order to assess recent and active proliferation after BALB/c skin grafting. We found that after BALB/c skin

grafting, the frequency of Ki67$^+$ cells increased by day 7 and peaked on day 10 relative to naive CD8$^+$ T cells in both the draining lymph nodes and the spleen (Figure 2F). At day 10 post-transplant, nearly all of the L^d QL9$^+$ CD44^{hi} CD8$^+$ T cells were Ki67$^+$ in both the draining lymph nodes and spleen (Figure 2F). The frequency of Ki67$^+$ CD8$^+$ T cells also peaked in the bulk CD8$^+$ T cell population at day 10 (Figure S1).

We tested the antigen specificity of the Ki67 expression among CD8$^+$ T cells by assessing L^d QL9 CD8$^+$ T cells in C57BL/6 mice after syngeneic C57BL/6 grafts or after third-party allogeneic C3H grafts. In naive mice, a fraction of CD8$^+$ T cells are CD44^{hi} because they have recently undergone homeostatic proliferation and/or are specific for microbes, so-called virtual memory cells.[28] Therefore, we evaluated the Ki67 staining among both CD44^{lo} and virtual memory CD44^{hi} CD8$^+$ T cells in ungrafted mice (Figure S2). Bulk CD44^{hi} CD8$^+$ T cells had an increased frequency of Ki67$^+$ in response to allogeneic BALB/c or C3H grafts relative to syngeneic C57BL/6 grafts (Figure S2). In contrast, L^d QL9$^+$ CD8$^+$ T cells had elevated Ki67$^+$ frequency in response to BALB/c skin grafts, and the frequency of Ki67$^+$ was similar among syngeneic C57BL/6, allogeneic third-party C3H, or virtual memory cells (Figure S2). Thus, as measured by both absolute numbers and Ki67$^+$ frequency, L^d QL9 tetramer-binding CD8$^+$ T cells respond specifically to endogenously presented antigen in BALB/c skin grafts.

Graft-specific CD8$^+$ T cells maintain clonal diversity during the peak effector response

Given that the L^d QL9-specific CD8$^+$ T cells are found at an elevated precursor frequency relative to CD8$^+$ T cell populations specific for non-transplant antigens (Figure 1G), yet underwent a relatively modest fold expansion after grafting (Figures 2A–2C), we sought to evaluate the clonal dynamics of this antigen-specific population. We used a multiplexed *TCRB* sequencing platform in order to evaluate the anti-graft CD8$^+$ T cell response in naive and effector graft-specific CD8$^+$ T cells. To identify a graft-specific *TCRB* signature, we sequenced fluorescence-activated cell sorted (FACS) naive CD44^{lo} L^d QL9$^+$ T cells from naive mice and effector CD44^{hi} L^d QL9$^+$ T cells from mice on day 10 post-BALB/c skin graft to compare with bulk (L^d QL9$^-$) CD8$^+$ T cells sorted into CD44^{lo} naive and CD44^{hi} effector populations (Figure 3A).

We found that CD44^{hi} L^d QL9$^+$ T cells had significantly less population diversity versus naive CD44^{lo} L^d QL9$^+$ T cells, consistent with greater oligoclonality after grafting (Figure 3B). In order to evaluate the dynamics of clones that were enriched in the CD44^{hi} L^d QL9$^+$ population, we used the TCRdist package, which identifies biochemically similar CDR3 sequences called meta-clonotypes, in antigen-specific T cell populations evaluated in comparison with background populations.[29] We identified 43 meta-clonotypes that were enriched over background in our samples (Table S1). Compared with the naive L^d QL9$^+$ population, we found that a greater number of the post-graft CD44^{hi} L^d QL9$^+$ meta-clonotypes were found to have medium expansion, large expansion, and hyperexpansion frequencies (Figure 3C). Interestingly, clones recovered from within the skin grafts on day 10 remained relatively polyclonal, and all grafts contained meta-clonotypes (Figure 3D).

We next evaluated the representation of meta-clonotypes across individual mice and found that 13 meta-clonotypes were convergent, which we defined as present in 75% or more

of the individual mice CD44^{hi} L^{d} QL9^{+} populations (Figure 3E). The defining amino acid sequences of these meta-clonotypes varied, although there was a preference for a glycine at position 5 and/or 6, which was present in 8 of 13 of the convergent meta-clonotypes. We evaluated the expression of the convergent meta-clonotypes and found that they were enriched in the L^{d} QL9^{+} CD8^{+} T cells at day 10 post-graft relative to naive populations (Figure 3F). In each mouse, at least one of the convergent meta-clonotypes was present (Figures 3G and 3H). However, we did not find an increased number of convergent meta-clonotypes in the unsorted peripheral blood or skin grafts (Figures 3G and 3H). Thus, these data demonstrate that after transplantation, CD8^{+} T cells responding to a single allogeneic antigen maintain high clonal diversity. However, there may be biochemical properties that govern CD8^{+} T cell recognition of allogeneic antigen.

A low frequency of CD8^{+} T$_{EFF}$ express KLRG-1 after grafting

A significant goal in transplantation is to identify acutely responding T cells in order to monitor the risk for, or the presence of, acute cellular graft rejection. In order to understand the function of graft-specific effector CD8^{+} T cells, we evaluated the phenotypic profile of L^{d} QL9^{+} effector CD8^{+} T cells (T$_{EFF}$), as defined by CD44^{hi} status. We first evaluated the expression of CXCR3 and CD62L, two surface receptors that have been shown to be important for post-infection T$_{EFF}$ function. We found that nearly all L^{d} QL9^{+} and bulk CD8^{+} T cells became CXCR3^{+} at day 10 and remained stable to a memory time point (Figures S3A–S3C). About half of these CXCR3^{+} T$_{EFF}$ lost CD62L expression, and this frequency of CD62L^{lo} cells was also stable from day 10 to 42 after skin grafting. Thus, while these markers are useful for identifying antigen-experienced CD8^{+} T cells after transplantation, they do not delineate acutely responding effectors.

The early CD8^{+} T cell response is often defined by the reciprocal expression of the CD127 (interleukin-7 receptor α [IL-7Rα]) and KLRG-1 receptors. In the first 1–2 weeks after infection, a significant portion (50%–70%) of T$_{EFF}$ transiently downregulate CD127 and become KLRG-1^{+}, and these cells are short lived and display potent effector functions.[14,30,31] We assessed the expression of CD127 and KLRG-1 among L^{d} QL9^{+} T$_{EFF}$ after grafting in both the spleen and the draining lymph nodes. In response to a BALB/c skin graft, a low frequency of CD127^{lo}KLRG1^{+} T$_{EFF}$ were induced among L^{d} QL9^{+} and bulk CD8^{+} T cells in the spleen, with a peak frequency at day 10 that declined precipitously at days 21 and 42 (Figures S3D and S3E). In the draining lymph node, a similarly low frequency of KLRG-1^{+} T$_{EFF}$ were found (Figures S3F and S3G). Thus, these data show that among graft-specific L^{d} QL9^{+} cells after transplantation, KLRG-1 expression does not define an abundant population of acutely responding T$_{EFF}$.

Expression of the activated CD43 glycoform is increased on a population of CD8^{+} T$_{EFF}$ after grafting

To better characterize the phenotypes of the CD8^{+} T$_{EFF}$ after grafting, we analyzed a high-parameter flow cytometry panel with canonical costimulatory and activation markers using dimensionality reduction analysis. We evaluated L^{d} QL9^{+} and bulk CD8^{+} T cells on days 0, 10, 21, and 42 after BALB/c skin grafting by clustering these populations with FlowSOM and ConsensusClusterPlus and visualized with uniform manifold approximation

and projection (UMAP) dimensionality reduction (Figures 4A and 4B). We evaluated the frequency of clusters and found four clusters that were enriched on day 10 relative to the other time points and three clusters that were enriched on both days 21 and 42 (Figure S4). We further evaluated day 10 enriched clusters, as these fit the profile of a short-lived effector population. All four day 10 clusters were $CD44^{hi}$, $Ki67^{+}$, $CXCR3^{hi}$, and $KLRG\text{-}1^{-}$ (Figure 4C). Interestingly, these clusters varied most in expression of CD62L and the activated glycoform of CD43 (identified by the antibody clone 1B11). While day 10 clusters 1 and 2 were $CD62L^{hi}CD43^{-}$, cluster 3 was $CD62L^{lo}CD43^{-}$, and cluster 4 was $CD62L^{lo}CD43^{+}$ (Figure 4C). Thus, these two surface receptors appear to represent dynamic populations within the T_{EFF} pool after grafting. In order to evaluate the expression of CD62L and CD43 after grafting, we performed manual gating on L^{d} $QL9^{+}$ and bulk $CD8^{+}$ T_{EFF}. We found that the frequency of $CD62L^{lo}CD43^{+}$ T_{EFF} increased at days 10 and 21 and were decreased at a memory day 42 time point (Figure 4D). The frequency of $CD62L^{lo}CD43^{+}$ $CD8^{+}$ T cells was also elevated at day 10 post-graft in the draining lymph nodes relative to naive mice (Figure 4E). Thus, activated CD43 expression defines a population of $CD62L^{lo}$ T_{EFF} that appear acutely after grafting and decline over time, fitting the kinetic profile of an acutely responding $CD8^{+}$ T_{EFF} population.

$CD43^{+}$ $CD8^{+}$ T_{EFF} display potent effector functions relative to $CD43^{-}$ T_{EFF} populations

CD43 is a transmembrane receptor that has been shown to impact intracellular signaling cascades, apoptosis, and T cell trafficking. However, the role of activated CD43 expression on $CD8^{+}$ T cells is not well understood in the context of transplantation. Thus, we next sought to assess whether $CD43^{+}$ T_{EFF} displayed competent effector functions relative to $CD43^{-}$ T_{EFF} populations. We grafted C57BL/6 mice with BALB/c skin and assessed $CD8^{+}$ T cells during the peak effector response (days 10–14; Figure 5A). We found that among the L^{d} $QL9^{+}$ cells, $CD43^{+}$ T_{EFF} expressed significantly higher levels of both granzyme B and T-Bet as compared with $CD62L^{hi}$ or $CD62L^{lo}$ $CD43^{-}$ T_{EFF} populations (Figures 5B and 5C). We assessed the capacity of these populations for cytokine production by stimulating $CD45.1^{+}$ T_{EFF} *ex vivo* with BALB/c splenocytes and found that nearly all of the interferon γ (IFN-γ) and tumor necrosis factor α (TNF-α) was produced by $CD43^{+}$ T_{EFF} and that the majority of these cells were double-cytokine producers (Figure 5D).

Activated CD43 expression is induced by antigen and inflammatory signals

Our data show that activated CD43 is induced after exposure to allogeneic BALB/c antigen *in vivo*, which entails exposure to both allogeneic antigen and inflammatory cytokines. As multiple studies have demonstrated that pathogen-induced inflammation impacts the development and function of $CD8^{+}$ T cell populations, we questioned whether inflammatory cytokines alone can drive the expression of activated CD43 during T cell priming.[14,32] To decouple transplant-induced inflammatory signals from allogeneic antigen, we grafted mice with allogeneic BALB/c skin, third-party allogeneic C3H skin, or syngeneic C57BL/6 skin. We found that allogeneic BALB/c or C3H skin grafts induced CD43 expression among bulk $CD8^{+}$ T cells (Figure 5E), and the frequency of $CD43^{+}$ cells was partly elevated among L^{d} $QL9^{+}$ $CD8^{+}$ T cells. Given that C3H grafting did not induce an increase in the number of $CD44^{hi}$ $CD8^{+}$ T cells (Figure 2B) or $Ki67^{+}$ cells (Figure S2), these data demonstrate a mechanism of bystander activation induced by allogeneic inflammation.

In order to more carefully evaluate the impact of inflammatory cytokines on CD43 expression, we activated OT-I T cells *in vitro* in the presence of individual inflammatory cytokines (Figure 5F). We used CellTrace Violet to assess the proliferation status of cells in culture. We included expression of Nur77, an orphan nuclear receptor whose expression level reflects the cumulative strength of antigen stimulation,[33,34] as a control for the overall level of activation of the cells in the presence of cytokines. We found that antigen stimulation alone induced CD43 and Nur77 expression (Figure 5G). The TLR9 agonist CpG, which has been shown to induce CD43 (1B11) expression,[35] increased CD43 expression more than antigen stimulation alone. Among inflammatory cytokines, we found that only IFN-α induced CD43 expression, while IFN-γ, IL-15, and IL-12 did not have an effect versus antigen stimulation alone (Figure 5G). The expression of Nur77 was not significantly impacted by the provision of any inflammatory cytokine. These results demonstrate that CD43 (1B11) expression is enhanced by antigen and can be augmented by type I IFN-mediated signaling.

CD43$^+$ T_{EFF} potently infiltrate allografts and mediate accelerated graft rejection

We wanted to assess whether the effector phenotype corresponded with an enhanced potency to mediate graft rejection *in vivo*. To isolate the impact of CD43 on T_{EFF}, we flow cytometrically sorted congenic CD45.1 CD44^{hi} CD8$^+$ T cells on days 10–14 post-BALB/c skin graft into CD43$^+$ and CD43$^-$ T_{EFF} (CD62L^{lo}) populations and adoptively transferred each into naive C57BL/6 mice who were subsequently grafted with BALB/c skin (Figure 6A). Using the magnetic bead enrichment technique for CD45.1, we recovered similar numbers of CD43$^+$ and CD43$^-$ T_{EFF} in the spleen on day 8 post-graft (Figure 6B). We evaluated the number of CD45.1$^+$ cells in BALB/c skin grafts and found a significantly greater number of sorted CD43$^+$CD45.1$^+$ CD8$^+$ T cells relative to CD43$^-$CD45.1$^+$ CD8$^+$ T cells (Figure 6C). This corresponded to a decrease in the endogenous CD8$^+$ T cells in the allografts (Figure 6C). The increased infiltration was reflected in faster graft rejection kinetics among the CD43$^+$ T_{EFF} group (Figure 6D). In contrast, mice transferred with CD43$^+$ or CD43$^-$ T_{EFF} had similar rejection kinetics of third-party allogeneic C3H skin grafts (mean survival time [MST] 13 and 14 days, respectively; Figure S5). Overall, these data demonstrate that CD43$^+$ T_{EFF} are potent mediators of graft rejection.

Costimulation blockade with CTLA-4 Ig does not inhibit CD8$^+$ T cells

Costimulation blockade with CTLA-4 immunoglobulin (Ig) or a biochemical derivative is used to treat autoimmune disease and to prevent transplant rejection in kidney transplant patients. In transplant patients, CTLA-4 Ig is associated with acute T cell-mediated rejection, and pre-clinical studies have shown that CD8$^+$ T cells are relatively resistant to CTLA-4 Ig.[36–38] We next evaluated the impact of CTLA-4 Ig on CD43$^+$ T_{EFF} relative to other T_{EFF}. We treated mice with CTLA-4 Ig in comparison with a control untreated group and analyzed CD8$^+$ T cells on day 10 after grafting with BALB/c skin grafts (Figure 7A). Consistent with prior studies, we found that CTLA-4 Ig reduced the proliferation of CD4$^+$ T_{EFF} but did not restrain bulk CD8$^+$ T_{EFF} populations (Figure S6A). Among graft-specific L^d QL9$^+$ CD8$^+$ T cells, CTLA-4 Ig reduced the frequency of CD44^{hi}CD62L^{lo} T_{EFF} and proliferative CD62L^{lo}Ki67$^+$ cells in the draining lymph nodes and the spleen (Figures S6B–S6E).

In order to evaluate the phenotype of $CD8^+$ T cells in the presence of CTLA-4 Ig, we performed UMAP and clustering analysis of L^d $QL9^+$ and bulk $CD8^+$ T cells in treated and control mice (Figure 7B). We found four clusters that were $CD44^{hi}$ T_{EFF} and evaluated the expression of costimulation receptors, activation markers, and functional markers (Figures 7B–7D). $CD44^{hi}$ clusters 2 and 3 had high CD43 (1B11) expression and were also $CD62L^{lo}$, $CXCR3^{hi}$, and $Ki67^+$. Interestingly, both had high expression of the costimulation receptor induced T cell costimulator (ICOS) (Figure 7D). Using manual gating, we evaluated whether the frequency of CD62L and CD43 T_{EFF} was impacted by CTLA-4 Ig treatment and found that all three populations were maintained at similar frequencies at day 10 between groups (Figure 7E). We next evaluated ICOS expression on CD43 versus CD62L T_{EFF} and found that ICOS expression was almost exclusively found on $CD62L^{lo}CD43^+$ T_{EFF} (Figure 7F). In order to assess whether ICOS costimulation provisioned functional signals in the context of graft rejection, we assessed the impact of ICOS blockade in combination with CTLA-4 Ig treatment. We found that anti-ICOS with CTLA-4 Ig prolonged graft survival versus CTLA-4 Ig or anti-ICOS alone (Figure 7G). Thus, ICOS represents a functional costimulation target that can be used to inhibit CTLA-4 Ig-resistant $CD8^+$ T cells.

DISCUSSION

$CD8^+$ T cells are thought to respond to allogeneic antigen primarily through the direct antigen presentation pathway, in which host $CD8^+$ T cells recognize donor MHC complexed with ubiquitous self-peptides.[39–41] Burrack et al. recently used MHC class II tetramers to show that $CD4^+$ T cells can respond to directly presented allogeneic antigen in a mouse model of skin grafting.[42] In this study, we build upon several elegant studies by Eisen and colleagues to study the $CD8^+$ T cell response directed against the H-$2L^d$ complexed with the self-peptide QL9, derived from α-ketoglutarate dehydrogenase. While this early work defined the biochemistry of the 2C TCR binding with L^d QL9 *in vitro,*[20–22,43–45] the *in vivo* immune $CD8^+$ T cell response directed at L^d QL9 has not been evaluated.

Thus, we sought to use the MHC class I tetramer enrichment approach to study L^d QL9-specific $CD8^+$ T cells. We found that at the peak of the immune response against BALB/c skin grafts, the majority of L^d $QL9^+$ T cells become $CD44^{hi}$ and that nearly all $CD44^{hi}$ L^d $QL9^+$ T cells are $Ki67^+$, providing strong evidence that the tetramer-binding T cells recognize endogenously presented L^d QL9 on graft tissue. This response was antigen specific, as L^d $QL9^+$ $CD8^+$ T cells did not expand in number or become $Ki67^+$ in response to syngeneic C57BL/6 grafts nor third-party allogeneic C3H skin grafts. Interestingly, while the QL9 peptide is a single amino acid extension of the parent 2C peptide, prior studies investigating the peptides recognized by the 2C TCR speculated that the QL9 was not detected on donor antigen-presenting cells due to technical limitations of peptide sequencing in acidic conditions.[21,44]

We found that the precursor frequency for L^d $QL9^+$ T cells is elevated compared with K^b OVA and D^b LCMV gp33, as well as compared with the published frequencies of other pathogen-specific antigens.[16–19] Prior studies estimating the precursor frequency of alloreactive T cells have relied on a wide variety of techniques, including *in vitro* stimulation for proliferation or cytokine production, and have relied on memory-containing T cell

populations and/or expanded T cell lines.[5,46–49] Thus, our findings using an MHC tetramer to directly visualize epitope-specific $CD8^+$ T cells significantly strengthens the knowledge about the precursor frequency of alloimmunity gained from these prior studies.

The biochemical nature of direct-pathway alloreactive T cells has remained the subject of debate. Prior work has attributed the recognition of allogeneic peptide-MHC complexes to poly specificity of the TCR itself, to peptide-independent recognition of peptide-MHC complexes, or to altered thymic selection of dual-TCR T cells.[5,24,26,50,51] A recent elegant study by Son et al. explored the importance of the self-peptide repertoire in shaping alloimmunity.[52] The authors found a critical role for the self-peptide repertoire in direct-pathway allogeneic $CD8^+$ T cell response such that perturbation of the peptide repertoire of allogeneic H-$2K^b$ complexes abrogated tolerance. We evaluated the requirement for the QL9 peptide in the responding alloreactive H-$2L^d$-specific $CD8^+$ T cells.

We found that L^d $QL9^+$ $CD8^+$ T cells did not simultaneously bind to H-$2L^d$ tetramers with either a biochemically related or an unrelated viral peptide and that $CD8^+$ T cells specific for other H2-L^d complexes did not increase in number in response to a BALB/c skin graft. These data demonstrate that the peptide is a major determining factor in the direct pathway of alloreactive $CD8^+$ T cells. Future work is needed to reconcile the alternate mechanisms for direct pathway recognition of allogeneic antigen and to further elucidate the peptide residues required for the L^d QL9-specific $CD8^+$ T cell response. In addition, future studies will need to further address the breadth of the anti-H-2^d alloimmune response, as Son et al. showed that the majority of the K^b-specific alloimmune response was dominated by only five peptide-MHC complexes.[52]

Our results provide a model in which alloreactive $CD8^+$ T cells exist at a high precursor frequency but undergo relatively weak clonal expansion. Consistent with this, *TCRB* sequencing of the L^d QL9-specific $CD8^+$ T cell response reveals a highly diverse response at the clonal level. While we identified biochemically similar group of convergent meta-clonotypes that expanded after grafting, the anti-graft $CD8^+$ T cell response remained diverse between individual animals. Interestingly, while we observed that the meta-clonotypes were present in graft tissue, the graft-infiltrating response was not dominated by the convergent clones at day 10 post-graft. It is not clear whether the $CD8^+$ T cell meta-clonotypes that expand in the secondary lymphoid organs preferentially enter the graft or if the graft tissue is infiltrated by predominantly polyclonal populations with private specificities. Monitoring the infiltration of cells into skin grafts is technically challenging, and future studies are needed to evaluate additional time points and gain a better understanding of the clonal properties and kinetics of the $CD8^+$ T cell infiltration into graft.

In contrast to pathogen-specific $CD8^+$ T cell responses at acute time points, we found that very few $CD8^+$ T_{EFF} expressed KLRG-1 after grafting. This highlights that the allogeneic priming environment has phenotypic consequences in shaping $CD8^+$ T cell responses and led us to carefully evaluate the post-graft $CD8^+$ T cell programming. Using a high-parameter flow cytometry panel to evaluate activation, costimulation, and proliferation markers, we found that a subset of L^d $QL9^+$ T_{EFF} express the activated glycoform of CD43 (1B11 clone).

The frequency CD43$^+$ T_{EFF} increased acutely after transplant, and these cells were potently cytotoxic relative to CD43$^-$ T_{EFF} populations.

CD43 is a transmembrane receptor with recognized intracellular signaling and adhesion functions.[53–55] CD43 is uniformly high on T cells, but a larger activated glycoform, defined by the 1B11 epitope, is selectively expressed in certain contexts.[56] Studies evaluating the role of CD43 in disease models have found varying and sometimes conflicting consequences. CD43-deficient CD8$^+$ T cells have been found to undergo a decreased rate of apoptosis during the contraction phase of the response to a virus[55] but have included increased levels of apoptosis in a model of sepsis.[57] Multiple studies have shown that CD43 is critical for trafficking into peripheral tissues.[53,55,58–60] Of note, the majority of studies have evaluated the function of CD43-sufficient versus -deficient strains, and less is known about the functional impact of CD43 1B11 glycoform expression on T cells. Future studies will be needed to evaluate the importance of CD43 1B11 expression on the function of T_{EFF} in the context of transplant, including the ability to traffic within secondary lymphoid tissue and into allografts.

Finally, we evaluated antigen-specific T_{EFF} in the presence of costimulation blockade with CTLA-4 Ig and found that the costimulatory receptor ICOS is selectively expressed on CD43$^+$ T_{EFF}. Blockade of ICOS prolonged graft survival, indicating that ICOS plays a functional role in the presence of CTLA-4 Ig treatment. ICOS has been implicated as an important costimulatory receptor in multiple T cell subsets and was recently shown to be important for the formation of resident memory CD8$^+$ T cells.[61] ICOS is attractive as a therapeutic target because it is selectively and transiently upregulated on CD43$^+$ T_{EFF} and thus represents a potentially selective way to inhibit allogeneic CD8$^+$ T cells during rejection. Currently, ICOS-blocking agents are in pre-clinical development for multiple diseases.[62,63]

Overall, by using an MHC tetramer-based approach, this study provides insight into the dynamics of the alloimmune CD8$^+$ T cell response, including the identification of a potent T_{EFF} phenotype. Future studies are needed to investigate the translational potential of these findings to inhibit graft-specific CD8$^+$ T cells in transplant patients.

Limitations of the study

This study utilized a fully allogeneic skin graft model to study alloimmunity. Skin grafts likely have lower levels of allogeneic antigen and/or distinct inflammatory properties than a transplanted visceral organ (e.g., heart or kidney) and could result in distinct adaptive immunologic response. In addition, transplanted skin is considered immunogenic due to a high content of resident immune cells, so findings of the phenotype and function of CD8$^+$ T cells should be validated in other graft models and in humans. While we were able to isolate CD8$^+$ T_{EFF} populations based on CD43 expression and show distinct functional properties relative to CD43$^-$ T_{EFF}, the biochemistry of CD43 receptor signaling is complex, and we did not show a requirement for this receptor for CD8$^+$ T_{EFF} function.

STAR★METHODS

RESOURCE AVAILABILITY

Lead contact—Further information and requests for resources and reagents should be directed to the lead contact, Scott Krummey (skrumme1@jhmi.edu)

Materials availability—This study did not generate new unique reagents.

Data and code availability

- *TCRB* sequencing data has been deposited in the Johns Hopkins Data Research Repository, and are publicly available as of the date of publication. DOIs are listed in the key resources table.
- All original code is available from the lead contact.
- Any additional information required to reanalyze the data reported in this paper is available from the lead contact.

EXPERIMENTAL MODEL AND SUBJECT DETAILS

Animals—C57BL/6J and C57BL/6J Ly5.2-Cr (CD45.1) strains were obtained from The Jackson Laboratory (Bar Harbor, Maine) and used at 6–12 weeks of age. Balb/cJ, C57Bl/6-Tg(TcraTcrb)1100Mjb/J (OT-I), and RAG1^{tm1Mom} (RAG1 knockout) were obtained from The Jackson Laboratory and bred at Emory University or Johns Hopkins University. All transplant experiments were conducted in age-matched hosts randomly assigned to experimental groups. This study was conducted in accordance with the recommendations in the Guide for the Care and Use of Laboratory Animals. The protocol was approved by the Animal Care and Use Committee at Emory University and Johns Hopkins University. Animals were housed in specific pathogen-free animal facilities at Emory University and Johns Hopkins University.

METHOD DETAILS

Skin grafting—Full-thickness tail and ear skins were transplanted onto the dorsal thorax of recipient mice and secured with adhesive bandages as previously described (Trambley et al., 1999). In some experiments, mice were treated with 250 μg/dose of CTLA-4 Ig (BioXCell) and anti-ICOS (BioXCell) via i.p. injection on day 0, 2, 4, and 6.

Skin graft T cell Isolation—Skin grafts were removed and minced into small pieces (<1 mm) and transferred into 500 μL Dulbecco's Modified Eagle Medium with 450 U/mL Collagenase Type II and 60 U/mL DNase-I (Worthington Biochemical). Samples were rocked for 2 h on a rocking shaker (150 rpm). Samples were then strained through a 70 mm filter into a 50 mL conical tube and washed with 5 mL cold PBS with 2% FBS. Cells were pelleted and stained with Live/Dead Near IR and antibodies for flow cytometry as described below.

MHC Tetramers and CD8$^+$ T cell enrichment—MHC tetramers with human β2-microglobulin specific for QL9 (H-2L^d QLSPFPFDL), LL9 (H-2L^d LSPFPFDLL), MuLV

(H-2L^d SPSYVYHQF) LCMV gp33 (H-2D^b KAVYFATC), and OVA (H-2K^b SIINFEKL) were obtained from the NIH Tetramer Core facility as biotinylated monomers. Tetramer production was performed by adding Streptavidin-RPE or -APC according to the core facility protocol. Tetramer enrichment was performed based on published protocols.[64] Briefly, single cell suspensions of splenocytes or lymphocytes were incubated with MHC tetramer (PE or APC), followed by incubation with anti-PE or anti-APC paramagnetic microbeads (Miltenyi), and enrichment over an LS column (Miltenyi). The column flow through was collected as the unbound fraction containing bulk CD8$^+$ T cells and the column bound fraction enriched for tetramer binding cells were stained for surface and intracellular antigens and analyzed by flow cytometry. Absolute cell counts were performed using CountBrite beads (BD Biosciences) or sample volume recorded by the Cytek Aurora.

Antibodies and Flow cytometry—Flow cytometry and magnetic enrichment were performed in 13 PBS (without Ca^{2+}/Mg^{2+}, pH 7.2), 0.25% BSA, 2 mM EDTA, and 0.09% azide. Single cell suspensions were incubated in 96-well U-bottom plates with the following antibodies for 30–60 min at room temperature: CD4, CD8, CD11c, F4/80, CD19, CD27, CD28, CD127, KLRG-1, CD43, CXCR3, CD62L, ICOS, CD44, CD62L. Intracellular staining was performed using the Transcription Factor Staining Kit (eBiosciences) and the following antigens: Ki67, Nur77, Granzyme B, T-Bet, IFN-γ, TNF-α. Dead cells were excluded with Live/Dead Aqua (Invitrogen), Live/Dead NIR Zombie (Biolegend), or propidium iodide (Invitrogen) according to manufacturer's instructions.

Ex vivo allogeneic Stimulation for cytokine production—Splenocytes and draining lymph node cells from CD45.1$^+$ mice grafted with Balb/c skin grafts 14 days prior were processed to single cell suspension and pooled. 1.5x10^6 CD45.1 cells were incubated with 2x10^6 Balb/c splenocytes in the presence of 1 mg/mL GolgiStop (Invitrogen) for 4–5 h at 37 C. Cells were collected and gated on CD45.1$^+$ CD8$^+$ T cells for intracellular cytokine analysis.

Flow cytometric cell sorting and adoptive transfer—Splenocytes and draining lymph nodes cells from CD45.1$^+$ mice grafted with Balb/c skin grafts 10–14 days prior were stained to identify effector CD62L^{lo}CD43$^+$ and CD62L^{lo}CD43$^-$ CD8$^+$ T cells. Cells were sorted on a MoFlo XDP. For skin graft survival experiments, 9x10^4 purified cells were transferred via tail vein into C57BL/6J mice. 2x10^5 purified cells were transferred for graft infiltration analysis. Mice were grafted the following day with Balb/c skin and monitored for graft survival.

In vitro OT-I stimulation—Naive OT-I splenocytes were stained with CellTrace Violet (Invitrogen) according to the manufacturer's instructions and plated in 24 well tissue culture plates at 3x10^6/well in in the presence of OT-I peptide (GenScript) and the following cytokines: CpG (3.125 μg/mL, Invivogen), IFN-α (Biolegend, 1.1 μg/mL), IL-12 (Biolegend, 10 ng/mL), IL-15 (Biolegend, 10 ng/mL), IFN-γ (Biolegend, 100 ng/mL). Cells were incubated in Complete R10 media comprised of RPMI 1640 with L-glutamine (Corning), 10% FBS, 100 mM HEPES, 500 μM β-mercaptoethanol, 100 U/mL penicillin/ stremptomycin at 37 C (5% CO_2) for 72 h prior to analysis by flow cytometry.

TCRB *sequencing (FR3AK-Seq) and analysis*—$CD8^+$ T cell populations from splenocytes and draining lymph nodes were flow cytometrically sorted from naive or post-Balb/c skin graft mice as described above. RNA from sorted cell pellets was isolated using the RNEasy Plus Mini kit (Qiagen) according to manufacturer instructions. RNA from peripheral blood was isolated after red blood cell lysis (eBiosciences). RNA from skin grafts was isolated from minced tissue using gentleMACS M columns and a gentleMACS Dissociator. RNA was stabilized using RNAprotect. cDNA was generated using the Superscript IV First-Strand Synthesis System kit per manufacturer protocol instructions. A normalized input of 200ng of RNA was used for each sample, or if the concentration was too low to reach 200ng, the maximum amount of RNA that could be input into the reaction was used. RNA corresponding to 1000 cells of the EL4 cell-line was used as a spike-in in all samples. cDNA samples were cleaned-up and concentrated using the Zymo Research ZR-96 DNA Clean and Concentrator kit (cat# D4023). 20 cycles of PCR1 were performed using the KAPA2G Fast Multiplex Mix and primers designed to encompass all mouse TCRBV alleles. 20 cycles of PCR2 was performed for sample barcoding. Sequencing was performed on an Illumina NextSeq. CDR3s were identified and quantified using MiXCR software (v 3.0.13), and the EL4 spike-in was used to normalize MiXCR clone counts.

Assembled clonotypes were imported and analyzed in R (4.1.1) via the immunarch (0.6.7) package. Clonotypes were categorized for expansion based on the relative frequency it represented in that sample using raw clone counts as follows: >1% hyper-expanded, 1%–0.1% large, 0.1%–0.01% medium, <0.01% small. Graphics were generated with ggplot2 (3.3.5). For any analysis, that required a defined v or j gene and there was an ambiguous result, the top hit was taken. Metaclonotypes were generated in python (3.8.12) using tcrdist3 (0.2.2). Data were imported using pandas (1.3.4). The enriched clonotypes consisted of sorted spleen cells, that were tetramer bound, and $CD44^{hi}$. The background set was generated from naive mouse blood samples (n = 14). A random sample of 280,000 of these clonotypes were generated with tcrsampler (0.1.9), and a v-j matched background of 280,000 clonotypes was generated with olga (1.2.4).

Flow cytometry analysis—In all analysis, $CD8^+$ T cells were identified as singlet events, Live/Dead $stain^-$, dump $gate^-$ (CD11c, F4/80, NK1.1, CD19), $CD4^-$, $CD8^+$ events. Manual gating was performed in Flowjo 10. Tetramer and bulk $CD8^+$ T_{EFF} are defined as $CD44^{hi}CD8^+$ T cells. For dimensionality reduction analysis, manually gated unbound $CD8^+$ T cells and bound fraction L^d $QL9^+$ $CD8^+$ T cells events were imported into R (4.1.1) through CytoML (2.40), flowWorkspace (4.4.0), and flowCore (2.4.0). Markers were transformed by hyperbolic arcsine with a cofactor of either 1000 or 6000 depending on the marker. The data were further analyzed using CATALYST (1.16.2) with FlowSOM (2.0.0) clustering and ConsensusClusterPlus (1.56.0) meta clustering. UMAP dimensionality reductions were generated with scatter (1.20.1). Visualizations were generated in ggplot2 (3.3.5) and ComplexHeatmap (2.8.0).

QUANTIFICATION AND STATISTICAL ANALYSIS

Statistical analysis—All data points represent individual mice, and where individual data points are not depicted the value of n is provided in the corresponding figure legend. For

analysis of absolute numbers and expression levels, paired or unpaired Student's t-tests (two-tailed) were performed between two groups; one-way or two-way ANOVA with multiple comparison tests were used to compare multiple groups. Log rank (Mantel-cox) test was used to evaluate graft survival between groups. *In vitro* CD43 and Nur77 expression data was normalized to the maximum MFI obtained for each marker in a given experiment. Error bars represent standard error measurements (SEM). Statistics were performed using GraphPad Prism 9. Significance was determined as *p < 0.05, **p < 0.01, ***p < 0.001, ****p < 0.0001.

Supplementary Material

Refer to Web version on PubMed Central for supplementary material.

ACKNOWLEDGMENTS

We thank members of the Mandy Ford Lab and the Johns Hopkins Department of Pathology for helpful review of the data. We thank Som Nanjappa and Whenhao Chen for helpful discussions and protocols. We appreciate Hao Zhang and the Bloomberg School of Public Health Flow Cytometry and Cell Sorting Core for excellent cell sorting and the NIH Tetramer Core Facility for tetramer reagents and technical advice. Figure graphics were created with BioRender.com. This work was supported by K99/R00 NIAID AI46271 (S.M.K.), a Transplant Immunology Research Network Fellowship Grant (S.M.K.), an American Society of Transplantation Research Network Career Transition Grant (S.M.K.), the Peter Buck Myositis Discovery Fund (H.B.L.), and S10OD026859 to support the Ross Flow Cytometry Core.

REFERENCES

1. Jameson SC, and Masopust D (2018). Understanding Subset Diversity in T Cell Memory. Immunity 48, 214–226. 10.1016/j.immuni.2018.02.010. [PubMed: 29466754]
2. Chung HK, McDonald B, and Kaech SM (2021). The architectural design of CD8+ T cell responses in acute and chronic infection: Parallel structures with divergent fates. J. Exp. Med 218, e20201730. 10.1084/jem.20201730. [PubMed: 33755719]
3. Ford ML (2016). T Cell Cosignaling Molecules in Transplantation. Immunity 44, 1020–1033. 10.1016/j.immuni.2016.04.012. [PubMed: 27192567]
4. Callemeyn J, Lamarthée B, Koenig A, Koshy P, Thaunat O, and Naesens M (2021). Allorecognition and the spectrum of kidney transplant rejection. Kidney Int 10.1016/j.kint.2021.11.029.
5. Felix NJ, Donermeyer DL, Horvath S, Walters JJ, Gross ML, Suri A, and Allen PM (2007). Alloreactive T cells respond specifically to multiple distinct peptide-MHC complexes. Nat. Immunol 8, 388–397. 10.1038/ni1446. [PubMed: 17322886]
6. Cherukuri A, Salama AD, Mehta R, Mohib K, Zheng L, Magee C, Harber M, Stauss H, Baker RJ, Tevar A, et al. (2021). Transitional B cell cytokines predict renal allograft outcomes. Sci. Transl. Med 13, eabe4929. 10.1126/scitranslmed.abe4929. [PubMed: 33627487]
7. Meier-Kriesche H-U, Ojo AO, Hanson JA, Cibrik DM, Punch JD, Leichtman AB, and Kaplan B (2000). Increased Impact of Acute Rejection on Chronic Allograft Failure in Recent Era. Transplantation 70. 10.1097/00007890-200010150-00018.
8. Cole EH, Johnston O, Rose CL, and Gill JS (2008). Impact of Acute Rejection and New-Onset Diabetes on Long-Term Transplant Graft and Patient Survival. Clin. J. Am. Soc. Nephrol 3, 814–821. 10.2215/CJN.04681107.
9. Dwyer GK, and Turnquist HR (2021). Untangling Local Pro-Inflammatory, Reparative, and Regulatory Damage-Associated Molecular-Patterns (DAMPs) Pathways to Improve Transplant Outcomes. Front. Immunol 12, 611910. 10.3389/fimmu.2021.611910. [PubMed: 33708206]
10. Colvin MM, Smith CA, Tullius SG, and Goldstein DR (2017). Aging and the immune response to organ transplantation. J. Clin. Invest 127, 2523–2529. 10.1172/JCI90601. [PubMed: 28504651]

11. Braza F, Brouard S, Chadban S, and Goldstein DR (2016). Role of TLRs and DAMPs in allograft inflammation and transplant outcomes. Nat. Rev. Nephrol 12, 281–290. 10.1038/nrneph.2016.41. [PubMed: 27026348]
12. Sarkar S, Kalia V, Haining WN, Konieczny BT, Subramaniam S, and Ahmed R (2008). Functional and genomic profiling of effector CD8 T cell subsets with distinct memory fates. J. Exp. Med 205, 625–640. 10.1084/jem.20071641. [PubMed: 18316415]
13. Herndler-Brandstetter D, Ishigame H, Shinnakasu R, Plajer V, Stecher C, Zhao J, Lietzenmayer M, Kroehling L, Takumi A, Kometani K, et al. (2018). KLRG1+ Effector CD8+ T Cells Lose KLRG1, Differentiate into All Memory T Cell Lineages, and Convey Enhanced Protective Immunity. Immunity 48, 716–729.e8. 10.1016/j.immuni.2018.03.015. [PubMed: 29625895]
14. Joshi NS, Cui W, Chandele A, Lee HK, Urso DR, Hagman J, Gapin L, and Kaech SM (2007). Inflammation Directs Memory Precursor and Short-Lived Effector CD8+ T Cell Fates via the Graded Expression of T-bet Transcription Factor. Immunity 27, 281–295. 10.1016/j.immuni.2007.07.010. [PubMed: 17723218]
15. Bozeman AM, Laurie SJ, Haridas D, Wagener ME, and Ford ML (2018). Transplantation preferentially induces a KLRG-1lo CD127hi differentiation program in antigen-specific CD8+ T cells. Transpl. Immunol 50, 34–42. 10.1016/j.trim.2018.06.003. [PubMed: 29885905]
16. Obar JJ, Khanna KM, and Lefrançois L (2008). Endogenous Naive CD8+ T Cell Precursor Frequency Regulates Primary and Memory Responses to Infection. Immunity 28, 859–869. 10.1016/j.immuni.2008.04.010. [PubMed: 18499487]
17. Kotturi MF, Scott I, Wolfe T, Peters B, Sidney J, Cheroutre H, von Herrath MG, Buchmeier MJ, Grey H, and Sette A (2008). Naive Precursor Frequencies and MHC Binding Rather Than the Degree of Epitope Diversity Shape CD8 $^{+}$ T Cell Immunodominance. J. Immunol 181, 2124–2133. 10.4049/jimmunol.181.3.2124. [PubMed: 18641351]
18. Haluszczak C, Akue AD, Hamilton SE, Johnson LDS, Pujanauski L, Teodorovic L, Jameson SC, and Kedl RM (2009). The antigen-specific CD8+ T cell repertoire in unimmunized mice includes memory phenotype cells bearing markers of homeostatic expansion. J. Exp. Med 206, 435–448. 10.1084/jem.20081829. [PubMed: 19188498]
19. Jenkins MK, and Moon JJ (2012). The Role of Naive T Cell Precursor Frequency and Recruitment in Dictating Immune Response Magnitude. J. Immunol 188, 4135–4140. 10.4049/jimmunol.1102661. [PubMed: 22517866]
20. Sykulev Y, Brunmark A, Tsomides TJ, Kageyama S, Jackson M, Peterson PA, and Eisen HN (1994). High-affinity reactions between antigen-specific T-cell receptors and peptides associated with allogeneic and syngeneic major histocompatibility complex class I proteins. Proc. Natl. Acad. Sci. USA 91, 11487–11491. 10.1073/pnas.91.24.11487. [PubMed: 7972089]
21. Chen J, Eisen HN, and Kranz DM (2003). A model T-cell receptor system for studying memory T-cell development. Microb. Infect 5, 233–240. 10.1016/S1286-4579(03)00016-9.
22. Udaka K, Tsomides TJ, and Eisen HN (1992). A naturally occurring peptide recognized by alloreactive CD8+ cytotoxic T lymphocytes in association with a class I MHC protein. Cell 69, 989–998. 10.1016/0092-8674(92)90617-L. [PubMed: 1606619]
23. Moon JJ, Chu HH, Pepper M, McSorley SJ, Jameson SC, Kedl RM, and Jenkins MK (2007). Naive CD4+ T Cell Frequency Varies for Different Epitopes and Predicts Repertoire Diversity and Response Magnitude. Immunity 27, 203–213. 10.1016/j.immuni.2007.07.007. [PubMed: 17707129]
24. Smith C, Miles JJ, and Khanna R (2012). Advances in Direct T-Cell Alloreactivity: Function, Avidity, Biophysics and Structure. Am. J. Transplant 12, 15–26. 10.1111/j.1600-6143.2011.03863.x. [PubMed: 22152064]
25. Karahan GE, Claas FHJ, and Heidt S (2021). Heterologous Immunity of Virus-Specific T Cells Leading to Alloreactivity: Possible Implications for Solid Organ Transplantation. Viruses 13, 2359. 10.3390/v13122359. [PubMed: 34960628]
26. Siu JHY, Surendrakumar V, Richards JA, and Pettigrew GJ (2018). T cell Allorecognition Pathways in Solid Organ Transplantation. Front. Immunol 9, 2548. 10.3389/fimmu.2018.02548. [PubMed: 30455697]

27. Marino J, Paster J, and Benichou G (2016). Allorecognition by T Lymphocytes and Allograft Rejection. Front. Immunol 7, 582. 10.3389/fimmu.2016.00582. [PubMed: 28018349]
28. White JT, Cross EW, and Kedl RM (2017). Antigen-inexperienced memory CD8+ T cells: where they come from and why we need them. Nat. Rev. Immunol 17, 391–400. 10.1038/nri.2017.34. [PubMed: 28480897]
29. Dash P, Fiore-Gartland AJ, Hertz T, Wang GC, Sharma S, Souquette A, Crawford JC, Clemens EB, Nguyen THO, Kedzierska K, et al. (2017). Quantifiable predictive features define epitope-specific T cell receptor repertoires. Nature 547, 89–93. 10.1038/nature22383. [PubMed: 28636592]
30. Milner JJ, Nguyen H, Omilusik K, Reina-Campos M, Tsai M, Toma C, Delpoux A, Boland BS, Hedrick SM, Chang JT, and Goldrath AW (2020). Delineation of a molecularly distinct terminally differentiated memory CD8 T cell population. Proc. Natl. Acad. Sci. USA 117, 25667–25678. 10.1073/pnas.2008571117. [PubMed: 32978300]
31. Herndler-Brandstetter D, Ishigame H, Shinnakasu R, Plajer V, Stecher C, Zhao J, Lietzenmayer M, Kroehling L, Takumi A, Kometani K, et al. (2018). KLRG1+ Effector CD8+ T Cells Lose KLRG1, Differentiate into All Memory T Cell Lineages, and Convey Enhanced Protective Immunity. Immunity 48, 716–729.e8. 10.1016/j.immuni.2018.03.015. [PubMed: 29625895]
32. Richer MJ, Pewe LL, Hancox LS, Hartwig SM, Varga SM, and Harty JT (2015). Inflammatory IL-15 is required for optimal memory T cell responses. J. Clin. Invest 125, 3477–3490. 10.1172/JCI81261. [PubMed: 26241055]
33. Krummey SM, Martinez RJ, Andargachew R, Liu D, Wagener M, Kohlmeier JE, Evavold BD, Larsen CP, and Ford ML (2016). Low-Affinity Memory CD8 $^{+}$ T Cells Mediate Robust Heterologous Immunity. J. Immunol 196, 2838–2846. 10.4049/jimmunol.1500639. [PubMed: 26864034]
34. Moran AE, Holzapfel KL, Xing Y, Cunningham NR, Maltzman JS, Punt J, and Hogquist KA (2011). T cell receptor signal strength in Treg and iNKT cell development demonstrated by a novel fluorescent reporter mouse. J. Exp. Med 208, 1279–1289. 10.1084/jem.20110308. [PubMed: 21606508]
35. Nolz JC, and Harty JT (2014). IL-15 regulates memory CD8+ T cell O-glycan synthesis and affects trafficking. J. Clin. Invest 124, 1013–1026. 10.1172/JCI72039. [PubMed: 24509081]
36. Crepeau RL, and Ford ML (2017). Challenges and opportunities in targeting the CD28/CTLA-4 pathway in transplantation and autoimmunity. Expet Opin. Biol. Ther 17, 1001–1012. 10.1080/14712598.2017.1333595.
37. Liu D, Krummey SM, Badell IR, Wagener M, Schneeweis LA, Stetsko DK, Suchard SJ, Nadler SG, and Ford ML (2014). 2B4 (CD244) induced by selective CD28 blockade functionally regulates allograft-specific CD8+ T cell responses. J. Exp. Med 211, 297–311. 10.1084/jem.20130902. [PubMed: 24493803]
38. Ford ML, Koehn BH, Wagener ME, Jiang W, Gangappa S, Pearson TC, and Larsen CP (2007). Antigen-specific precursor frequency impacts T cell proliferation, differentiation, and requirement for costimulation. J. Exp. Med 204, 299–309. 10.1084/jem.20062319. [PubMed: 17261633]
39. Siu JHY, Surendrakumar V, Richards JA, and Pettigrew GJ (2018). T cell Allorecognition Pathways in Solid Organ Transplantation. Front. Immunol 9, 2548. 10.3389/fimmu.2018.02548. [PubMed: 30455697]
40. Harper SJF, Ali JM, Wlodek E, Negus MC, Harper IG, Chhabra M, Qureshi MS, Mallik M, Bolton E, Bradley JA, and Pettigrew GJ (2015). CD8 T-cell recognition of acquired alloantigen promotes acute allograft rejection. Proc. Natl. Acad. Sci. USA 112, 12788–12793. 10.1073/pnas.1513533112. [PubMed: 26420874]
41. Young JS, McIntosh C, Alegre M-L, and Chong AS (2017). Evolving Approaches in the Identification of Allograft-Reactive T and B Cells in Mice and Humans. Transplantation 101, 2671–2681. 10.1097/TP.0000000000001847. [PubMed: 28604446]
42. Burrack AL, Malhotra D, Dileepan T, Osum KC, Swanson LA, Fife BT, and Jenkins MK (2018). Cutting Edge: Allograft Rejection Is Associated with Weak T Cell Responses to Many Different Graft Leukocyte-Derived Peptides. J. Immunol 200, 477–482. 10.4049/jimmunol.1701434. [PubMed: 29255075]

43. Sykulev Y, Joo M, Vturina I, Tsomides TJ, and Eisen HN (1996). Evidence that a Single Peptide–MHC Complex on a Target Cell Can Elicit a Cytolytic T Cell Response. Immunity 4, 565–571. 10.1016/S1074-7613(00)80483-5. [PubMed: 8673703]
44. Sykulev Y, Brunmark A, Jackson M, Cohen RJ, Peterson PA, and Eisen HN (1994). Kinetics and affinity of reactions between an antigen-specific T cell receptor and peptide-MHC complexes. Immunity 1, 15–22. 10.1016/1074-7613(94)90005-1. [PubMed: 7889394]
45. Udaka K, Wiesmüller KH, Kienle S, Jung G, and Walden P (1996). Self-MHC-restricted peptides recognized by an alloreactive T lymphocyte clone. J. Immunol 157, 670–678. [PubMed: 8752916]
46. Macedo C, Orkis EA, Popescu I, Elinoff BD, Zeevi A, Shapiro R, Lakkis FG, and Metes D (2009). Contribution of Naïve and Memory T-Cell Populations to the Human Alloimmune Response. Am. J. Transplant 9, 2057–2066. 10.1111/j.1600-6143.2009.02742.x. [PubMed: 19624567]
47. Suchin EJ, Langmuir PB, Palmer E, Sayegh MH, Wells AD, and Turka LA (2001). Quantifying the Frequency of Alloreactive T Cells In Vivo: New Answers to an Old Question. J. Immunol 166, 973–981. 10.4049/jimmunol.166.2.973. [PubMed: 11145675]
48. Heeger PS, Greenspan NS, Kuhlenschmidt S, Dejelo C, Hricik DE, Schulak JA, and Tary-Lehmann M (1999). Pretransplant frequency of donor-specific, IFN-gamma-producing lymphocytes is a manifestation of immunologic memory and correlates with the risk of posttransplant rejection episodes. J. Immunol 163, 2267–2275. [PubMed: 10438971]
49. Amir AL, D'Orsogna LJA, Roelen DL, van Loenen MM, Hagedoorn RS, de Boer R, van der Hoorn MAWG, Kester MGD, Doxiadis IIN, Falkenburg JHF, et al. (2010). Allo-HLA reactivity of virus-specific memory T cells is common. Blood 115, 3146–3157. 10.1182/blood-2009-07-234906. [PubMed: 20160165]
50. Wucherpfennig KW, Allen PM, Celada F, Cohen IR, De Boer R, Garcia KC, Goldstein B, Greenspan R, Hafler D, Hodgkin P, et al. (2007). Polyspecificity of T cell and B cell receptor recognition. Semin. Immunol 19, 216–224. 10.1016/j.smim.2007.02.012. [PubMed: 17398114]
51. Balakrishnan A, and Morris GP (2016). The highly alloreactive nature of dual TCR T cells. Curr. Opin. Organ Transplant 21, 22–28. 10.1097/MOT.0000000000000261. [PubMed: 26555233]
52. Son ET, Faridi P, Paul-Heng M, Leong ML, English K, Ramarathinam SH, Braun A, Dudek NL, Alexander IE, Lisowski L, et al. (2021). The self-peptide repertoire plays a critical role in transplant tolerance induction. J. Clin. Invest 131, e146771. 10.1172/JCI146771. [PubMed: 34428180]
53. Mody PD, Cannon JL, Bandukwala HS, Blaine KM, Schilling AB, Swier K, and Sperling AI (2007). Signaling through CD43 regulates CD4 T-cell trafficking. Blood 110, 2974–2982. 10.1182/blood-2007-01-065276. [PubMed: 17638845]
54. Sperling AI, Green JM, Mosley RL, Smith PL, DiPaolo RJ, Klein JR, Bluestone JA, and Thompson CB (1995). CD43 is a murine T cell costimulatory receptor that functions independently of CD28. J. Exp. Med 182, 139–146. 10.1084/jem.182.1.139. [PubMed: 7790813]
55. Onami TM, Harrington LE, Williams MA, Galvan M, Larsen CP, Pearson TC, Manjunath N, Baum LG, Pearce BD, and Ahmed R (2002). Dynamic Regulation of T Cell Immunity by CD43. J. Immunol 168, 6022–6031. 10.4049/jimmunol.168.12.6022. [PubMed: 12055210]
56. Clark MC, and Baum LG (2012). T cells modulate glycans on CD43 and CD45 during development and activation, signal regulation, and survival. Ann. N. Y. Acad. Sci 1253, 58–67. 10.1111/j.1749-6632.2011.06304.x. [PubMed: 22288421]
57. Fay KT, Chihade DB, Chen C-W, Klingensmith NJ, Lyons JD, Ramonell K, Liang Z, Coopersmith CM, and Ford ML (2018). Increased mortality in CD43-deficient mice during sepsis. PLoS One 13, e0202656. 10.1371/journal.pone.0202656. [PubMed: 30226896]
58. Ford ML, Onami TM, Sperling AI, Ahmed R, and Evavold BD (2003). CD43 Modulates Severity and Onset of Experimental Autoimmune Encephalomyelitis. J. Immunol 171, 6527–6533. 10.4049/jimmunol.171.12.6527. [PubMed: 14662853]
59. Cannon JL, Mody PD, Blaine KM, Chen EJ, Nelson AD, Sayles LJ, Moore TV, Clay BS, Dulin NO, Shilling RA, et al. (2011). CD43 interaction with ezrin-radixin-moesin (ERM) proteins regulates T-cell trafficking and CD43 phosphorylation. Mol. Biol. Cell 22, 954–963. 10.1091/mbc.e10-07-0586. [PubMed: 21289089]

60. Ford ML, and Evavold BD (2006). Modulation of MOG 37-50-specific CD8+ T cell activation and expansion by CD43. Cell. Immunol 240, 53–61. 10.1016/j.cellimm.2006.06.007. [PubMed: 16890924]

61. Peng C, Huggins MA, Wanhainen KM, Knutson TP, Lu H, Georgiev H, Mittelsteadt KL, Jarjour NN, Wang H, Hogquist KA, et al. (2022). Engagement of the costimulatory molecule ICOS in tissues promotes establishment of CD8+ tissue-resident memory T cells. Immunity 55, 98–114.e5. 10.1016/j.immuni.2021.11.017. [PubMed: 34932944]

62. Solinas C, Gu-Trantien C, and Willard-Gallo K (2020). The rationale behind targeting the ICOS-ICOS ligand costimulatory pathway in cancer immunotherapy. ESMO Open 5, e000544. 10.1136/es-moopen-2019-000544. [PubMed: 32516116]

63. Adom D, Dillon SR, Yang J, Liu H, Ramadan A, Kushekhar K, Hund S, Albright A, Kirksey M, Adeniyan T, et al. (2020). ICOSL $^{+}$ plasmacytoid dendritic cells as inducer of graft-versus-host disease, responsive to a dual ICOS/CD28 antagonist. Sci. Transl. Med 12, eaay4799. 10.1126/scitranslmed.aay4799. [PubMed: 33028709]

64. Moon JJ, Chu HH, Hataye J, Pagán AJ, Pepper M, McLachlan JB, Zell T, and Jenkins MK (2009). Tracking epitope-specific T cells. Nat. Protoc 4, 565–581. 10.1038/nprot.2009.9. [PubMed: 19373228]

Highlights

- $CD8^+$ T cells specific for the L^d $QL9^+$ epitope respond to allogeneic skin grafts
- Graft-specific $CD8^+$ T cells express activated CD43 during acute rejection
- $CD43^+$ $CD8^+$ T cells are potent effectors that rapidly infiltrate graft tissue
- CD28 blockade resistance may be mediated through ICOS costimulation on $CD43^+$ T_{EFF}

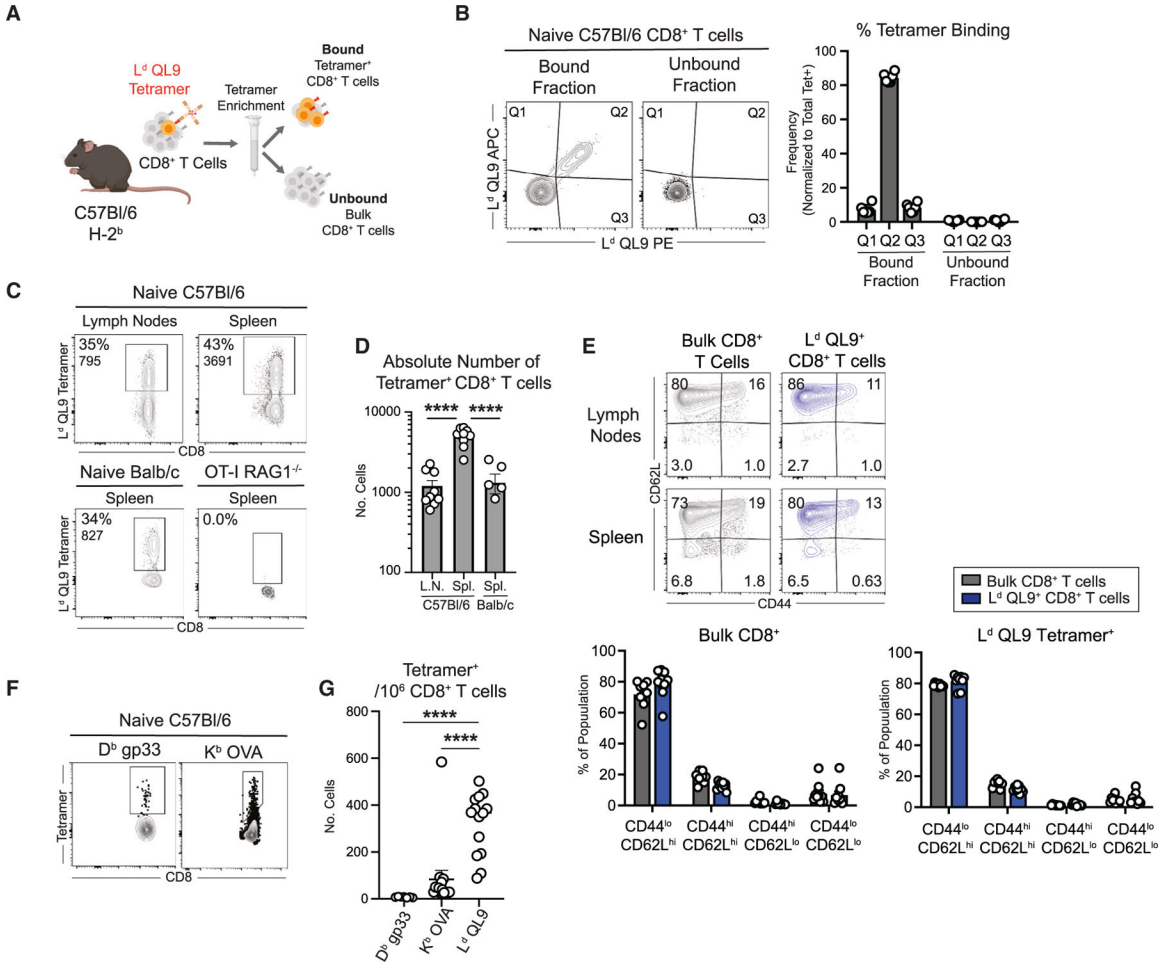

Figure 1. H-2L^{d} QL9 tetramers identify a population of naive CD8^{+} T cells at elevated precursor frequency

(A) Single-cell suspensions of lymph node or spleen tissue were incubated with MHC class I tetramers and enriched using magnetic beads specific for the tetramer fluorophores, creating column bound tetramer-enriched and unbound bulk CD8^{+} T cell fractions for analysis.

(B) Representative flow cytometry plots and summary data depicting the frequency of CD8^{+} T cells binding to L^{d} QL9 PE and L^{d} QL9 APC tetramers in the bound and unbound fractions.

(C) Representative flow cytometry plots of L^{d} QL9 tetramer staining in naive C57BL/6 spleen, C57BL/6 lymph nodes, BALB/c spleen, or OT-I *RAG1*$^{-/-}$ spleen.

(D) Absolute numbers of L^{d} QL9 tetramer-binding CD8^{+} T cells in the naive C57BL/6 lymph nodes, C57BL/6 spleen, or BALB/c spleen.

(E) Representative flow cytometry plots and summary data depicting the phenotype of L^{d} QL9 tetramer-binding CD8^{+} T cells in the lymph nodes and spleen.

(F) Representative flow cytometry plots of D^{b} LCMV gp33 and K^{b} OVA tetramer-binding CD8^{+} T cells.

(G) Number of D^{b} LCMV gp33, K^{b} OVA, and L^{d} QL9 tetramer-binding cells per million CD8^{+} T cells.

Each point depicts an individual mouse. Summary data depict pooled results from (B) 3 independent experiments (n = 6/group), (D and E) 2 independent experiments (n = 5–9/group), or (G) 2 independent experiments (n = 7–14/group). Statistical analyses performed using (D) Student's unpaired t test (two-tailed) or (G) one-way ANOVA with Dunnett's multiple comparisons test. Error bars depict SEM. ****$p < 0.0001$.

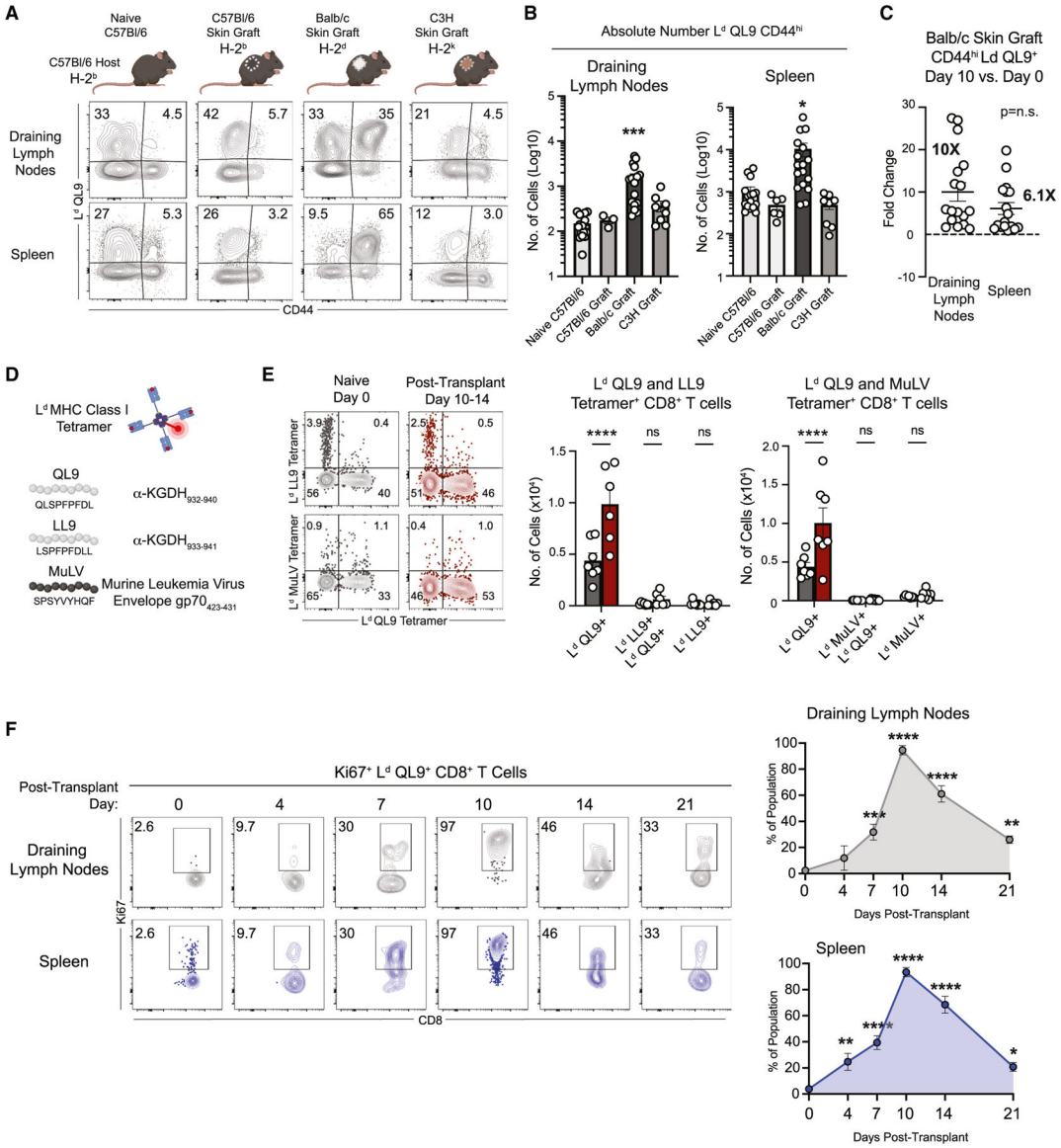

Figure 2. H-2L^{d} QL9^{+} CD8^{+} T cell expansion is dependent on H-2L^{d} expression and is largely peptide dependent

(A) C57BL/6 mice were grafted with H-2^{b} C57BL/6, H-2^{d} BALB/c, or H-2^{k} C3H skin. Representative flow cytometry plots depict the frequency of CD44^{hi} and CD44^{lo} among L^{d} QL9^{+} CD8^{+} T cells.

(B) Absolute numbers of CD8^{+} T cells from naive or day 10–14 post-graft mice in the draining lymph nodes and spleen.

(C) Fold change of the number of L^{d} QL9^{+} CD8^{+} T cells on day 10 post-BALB/c graft relative to day 0 in the draining lymph nodes or spleen.

(D) Schematic of MHC class I H-2L^{d} tetramers containing either QL9, LL9, or MuLV peptides.

(E) Left, representative flow plots depicting the bound fraction of CD8^{+} T cells in the spleen of C57BL/6 mice after BALB/c skin grafting. Right, absolute numbers of CD8^{+} T cells binding the indicated individual H-2L^{d} tetramers or both tetramers.

(F) Representative flow cytometry plots and summary data depict the frequency of L^d $QL9^+$ $CD44^{hi}$ and $CD44^{lo}$ $CD8^+$ T cells that are $Ki67^+$ from the spleen and draining lymph nodes post-BALB/c skin graft.

Each data point depicts an individual mouse. Summary data depict pooled data from (B) 2–4 independent experiments (n = 8–17/group), (C) 4 independent experiments (n = 12–17/group), (E) 2 independent experiments (6–7/group), or (F) 2–3 independent experiments (6–10/group). Statistical analyses performed using (B) one-way ANOVA with Sidak's multiple comparisons test, (E) mixed-effects ANOVA with Sidak's multiple comparisons test, or (F) one-way ANOVA with Dunnett's multiple comparisons test versus day 0. Error bars depict SEM. *p < 0.05, **p < 0.01, ***p < 0.001, ****p < 0.0001.

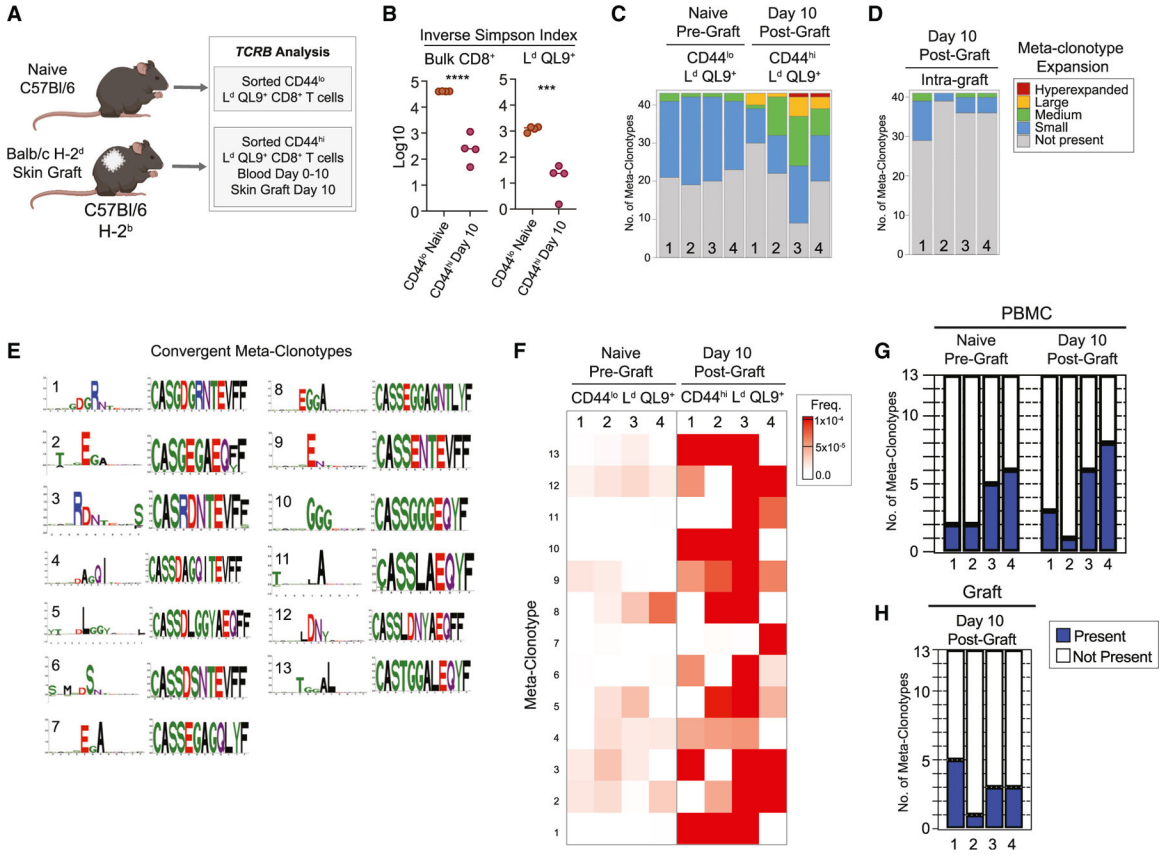

Figure 3. Graft-specific CD8$^+$ T cells maintain clonal diversity throughout the primary effector response

(A) C57BL/6 mice were grafted with BALB/c skin grafts, and multiple tissues were collected. Splenic CD8$^+$ T cell populations were flow cytometrically sorted based on L^d QL9 binding and CD44 expression.

(B) Inverse Simpson index for naive CD44^{lo} and day 10 CD44^{hi} T_{EFF} populations are depicted.

(C) Frequency of meta-clonotypes in each sample that are defined as hyperexpanded (>1%), large (0.1%–1%), medium (0.01%–0.1%), or small (<0.01%) or are not present.

(D) Frequency of meta-clonotypes defined as in (C), found in the skin graft tissue on day 10.

(E) CDR3 sequences from 13 convergent meta-clonotypes. The left TCR logo is scaled by per-column relative entropy to background population. The right TCR logo depicts the full meta-clonotype CDR3 sequence.

(F) Frequency of meta-clonotypes present in the splenic CD44^{lo} and CD44^{hi} L^d QL9$^+$ populations.

(G and H) Number of meta-clonotypes present in peripheral blood mononuclear cells (PBMCs) and graft tissue at the depicted time points.

Each data point depicts an individual mouse. Statistical analysis performed using unpaired Student's t test. Error bars depict SEM. ***p < 0.001, ****p < 0.0001.

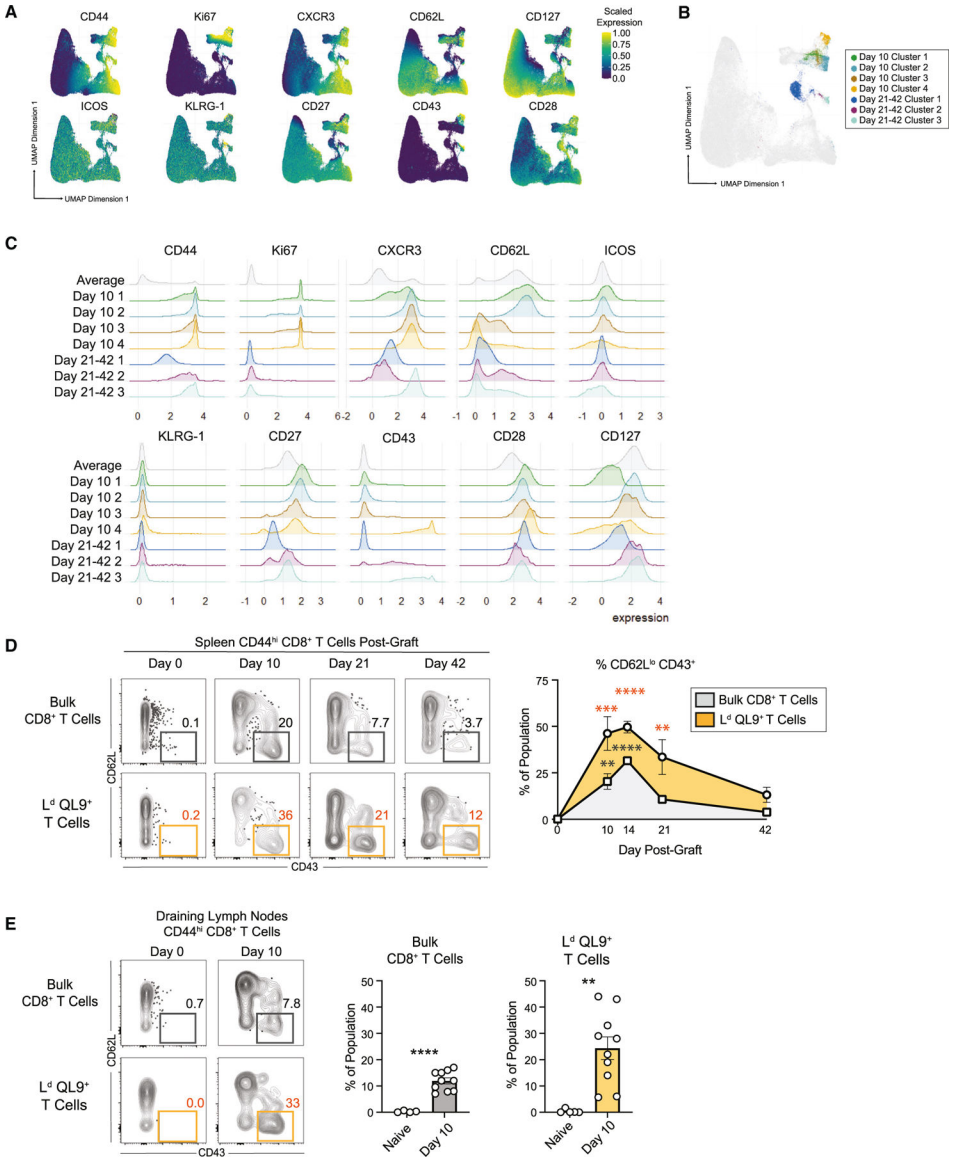

Figure 4. CD8$^+$ T cells differentiate into CD43$^+$ T$_{EFF}$ populations that peak early after grafting

C57BL/6 mice were grafted with H-2^d BALB/c skin, and the frequency of L^d QL9$^+$ and bulk CD8$^+$ T cells was assessed in the spleen at the indicated time points.

(A) UMAP of costimulation and activation markers from day 0, 10, 21, and 42 post-graft CD8$^+$ T cell populations.

(B) UMAP depicting day 10 and day 21/42 enriched clusters.

(C) Histograms depicting expression of individual markers in day 10 and day 21/42 enriched clusters.

(D) Expression of CD43 and CD62L on CD8$^+$ T cell populations at days 0, 10, 21, and 42 post-graft in the spleen.

(E) Expression of CD43 and CD62L on CD44^{hi} CD8$^+$ T cell populations at day 10 in the draining lymph nodes.

Each data point depicts an individual mouse. Summary data depict pooled results from (A–C) one independent experiment (n = 4 mice/group) or (D–E) 2–3 independent experiments (n = 5–10 mice/group). Statistics performed by (B, C, and E) one-way ANOVA with Dunnett's multiple comparison's test or (E) unpaired Student's t test. Error bars depict SEM. **p < 0.01, ***p < 0.001, ****p < 0.0001.

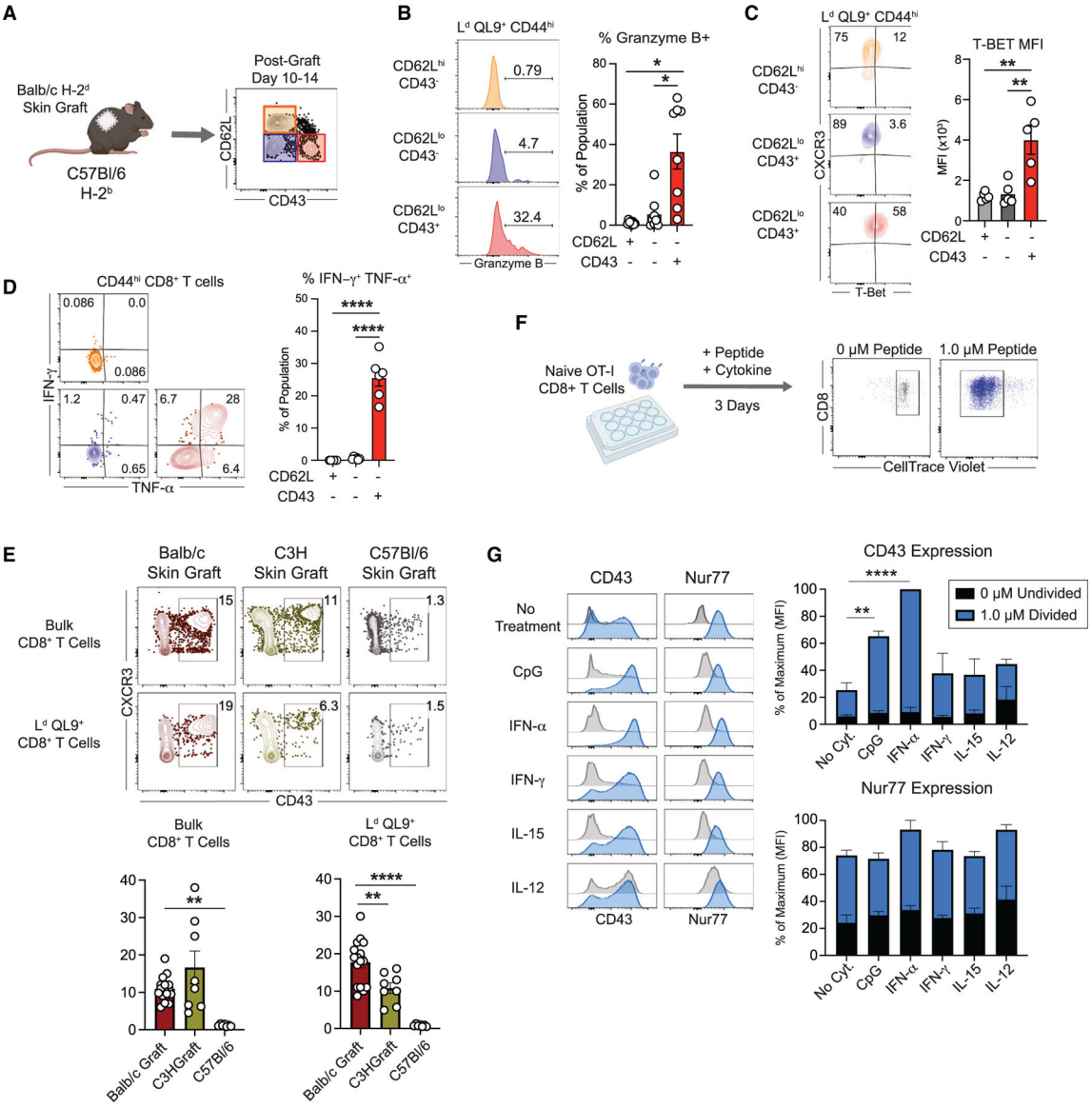

Figure 5. CD43$^+$ T_{EFF} display potent effector functions and can differentiate in response to inflammatory cytokines

(A–D) C57BL/6 mice were grafted with H-2^d BALB/c skin, and L^d QL9$^+$ and bulk CD8$^+$ T cells were assessed in the spleen at days 10–14 post-graft.

(B and C) Representative flow cytometry plots and summary data of (B) granzyme B$^+$ cells and (C) T-BET$^+$ cells in the indicated CD8$^+$ T_{EFF} populations.

(D) Post-graft effectors were stimulated *in vitro* for 5 h with BALB/c splenocytes, and the frequency of IFN-γ- and TNF-α-producing cells was assessed.

(E) Frequency of CD43$^+$ cells among bulk and L^d QL9$^+$ CD44^{hi} CD8$^+$ T_{EFF} in the spleen on days 10–14 after H-2^d BALB/c, H-2^k C3H, or H-2^b C57BL/6 skin grafts.

(F) OT-I CD8$^+$ T cells were labeled with CellTrace Violet and stimulated *in vitro* for 3 days in the presence of 0 (unstimulated) or 1 μM OVA peptide and the indicated cytokine.

(G) Histograms depicting the expression of CD43 and Nur77 on undivided unstimulated or 1 μM peptide divided populations. For each individual experiment, the mean fluorescence intensity (MFI) was normalized to the maximum value of CD43 or Nur77.

Each data point depicts an individual mouse. Summary data depict pooled results from (B–D) 2 independent experiments (n = 5–8 mice/group), (E) 2–4 independent experiments (n = 7–16 mice/group), or (G) 3 independent experiments with an individual mouse. Statistical analyses performed by (B–D) one-way ANOVA with Tukey's multiple comparisons test or (E and G) two-way ANOVA with Dunnett's multiple comparisons test versus (E) BALB/c graft or (G) no cytokine. Error bars depict SEM. *$p < 0.05$, **$p < 0.01$, ***$p < 0.001$, ****$p < 0.0001$.

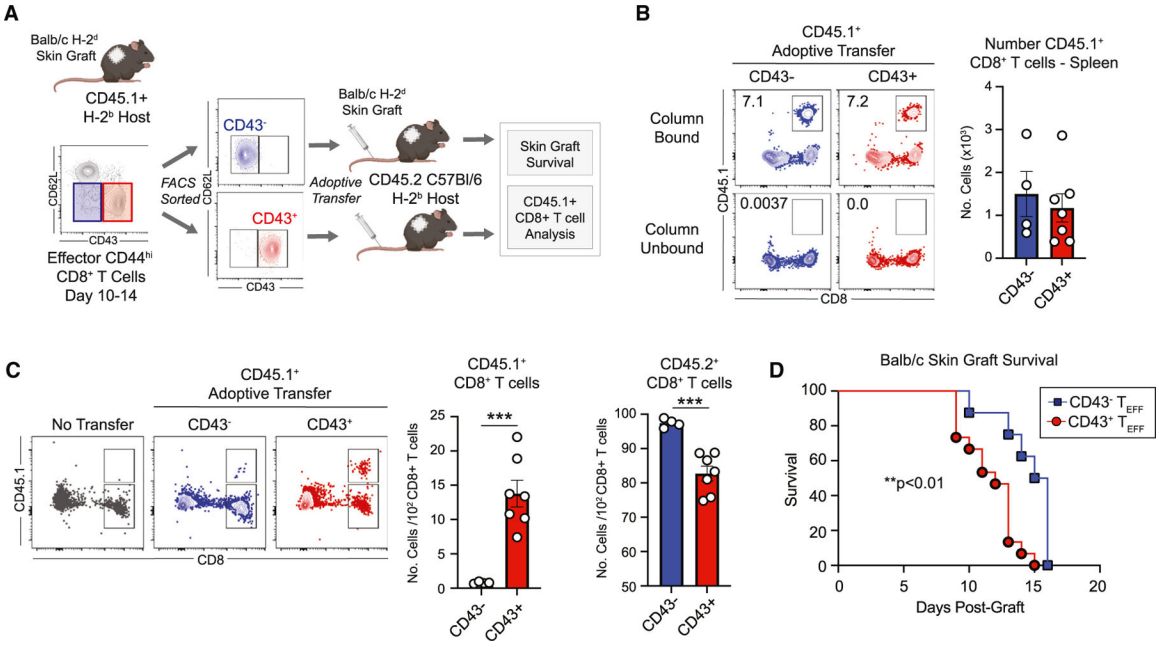

Figure 6. CD43$^+$ T_{EFF} rapidly infiltrate allografts and mediate accelerated graft rejection

(A) CD45.1$^+$ H-2^b mice were grafted with H-2^d BALB/c skin, and on days 10–14, CD8$^+$ T cells were FACS into CD44^{hi}CD62L^{lo} CD43$^+$ and CD43$^-$ CD8$^+$ T cell populations and adoptively transferred into naive C57BL/6 CD45.2 hosts. The following day, BALB/c skin grafts were provided.

(B) Transferred CD45.1$^+$ T cells were assessed using magnetic bead enrichment. Representative flow cytometry plots and summary data of CD45.1$^+$ CD8$^+$ T cells on day 8 post-graft in the spleen.

(C) Representative flow cytometry plots and absolute number of transferred CD45.1$^+$ and host CD45.2$^+$ CD8$^+$ T cells recovered from skin allografts.

(D) Graft survival analysis of C57BL/6 hosts transferred with CD45.1$^+$ CD8$^+$ T cell populations described in (A).

Each data point depicts an individual mouse. Summary data depict pooled results from (B and C) 4 independent experiments (n = 4–7 mice/group) or (D) 2 independent experiments (n = 7–15/group). Statistical analyses performed by (B–D) one-way ANOVA with Tukey's multiple comparisons test or (C) log-rank (Mantel-Cox) test. Error bars depict SEM. *p < 0.05, **p < 0.01, ****p < 0.0001.

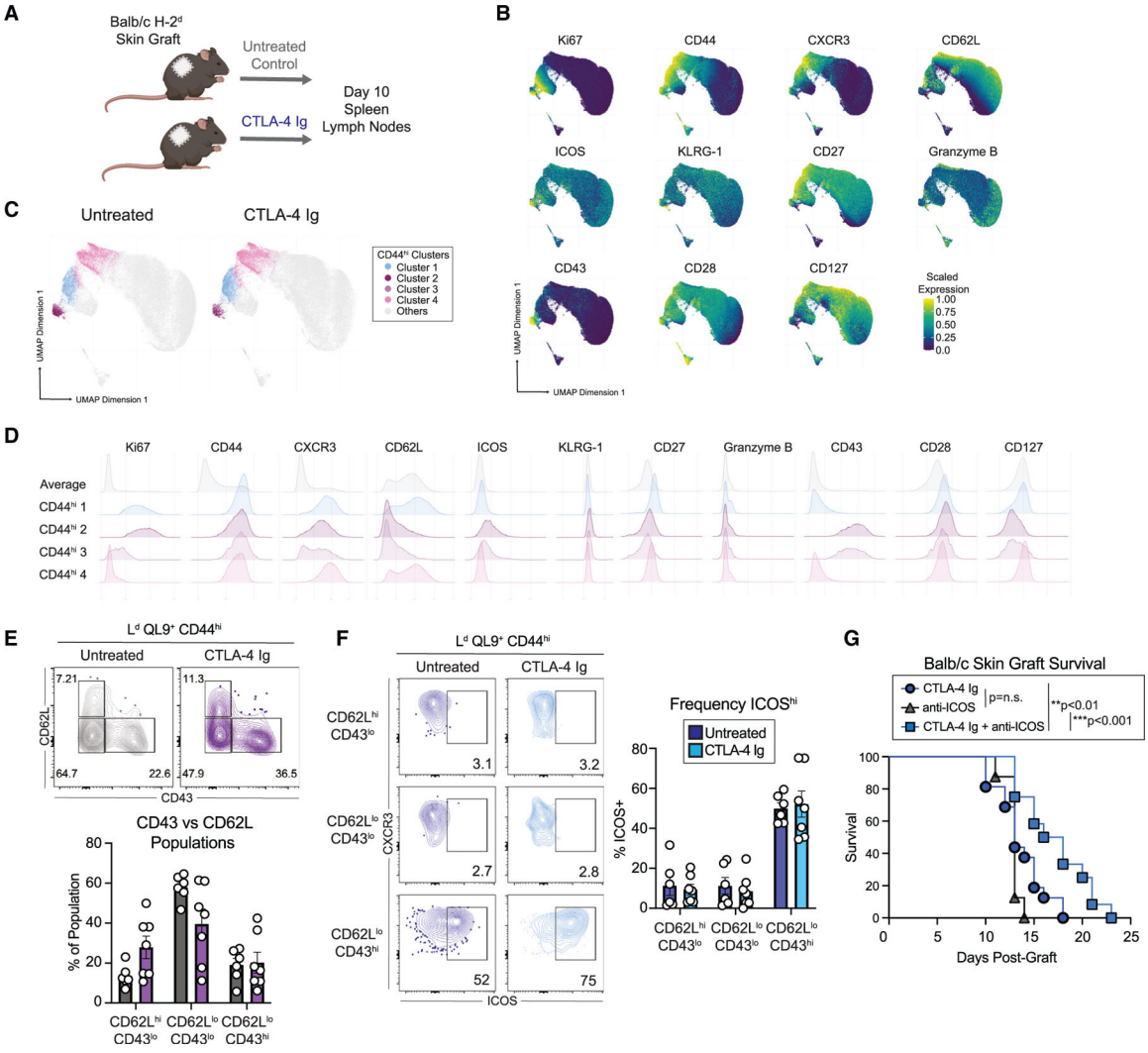

Figure 7. ICOS expression is induced on CD43^{+} T_{EFF}, and ICOS blockade prolongs graft survival

(A) Experimental schematic depicting the treatment of C57BL/6 mice grafted with H-2^{d} BALB/c skin and treated with CTLA-4 Ig.

(B) UMAP expression analysis of day 10 post-graft L^{d} QL9^{+} and bulk CD8^{+} T cells in the spleen in mice untreated or treated with CTLA-4 Ig.

(C) UMAP depicting four CD44^{hi} clusters.

(D) Histograms of proteins used in UMAP analysis for four CD44^{hi} clusters and the average of all samples.

(E) Representative flow cytometry plots and summary data depicting the frequency of CD62L- and CD43-expressing effector populations in the spleen on day 10 post-graft in mice.

(F) Expression of ICOS on CD8^{+} T_{EFF} populations in CTLA-4 Ig and control mice.

(G) Graft survival of C57BL/6 mice treated with CTLA-4 Ig, anti-ICOS, or CTLA-4 Ig and anti-ICOS and grafted with a BALB/c skin graft.

Each data point depicts an individual mouse. Summary data depict pooled results from (E and F) 2 independent experiments (n = 6–7 mice/group) or (G) 3 independent experiments (n = 8–16/group). Statistical analyses performed by (E and F) two-way ANOVA with Tukey's multiple comparisons test or (G) log-rank (Mantel-Cox) test. Error bars depict SEM. **p < 0.01, ***p < 0.001.

KEY RESOURCES TABLE

REAGENT or RESOURCE	SOURCE	IDENTIFIER
Antibodies		
Anti-mouse CD11c AF488 (clone N418)	Biolegend	Cat# 117313; RRID: AB_492849
Anti-mouse CD11c AF647 (clone N418)	Biolegend	Cat# 117312; RRID: AB_389328
Anti-mouse CD127 PE-Dazzle594 (clone A7R34)	Biolegend	Cat# 135032; RRID: AB_2564217
Anti-mouse CD19 AF488 (clone 6D5)	Biolegend	Cat# 115524; RRID: AB_493339
Anti-mouse CD19 AF647 (clone 6D5)	Biolegend	Cat# 115522; RRID: AB_389329
Anti-mouse CD27 BV785 (clone LG.3A10)	Biolegend	Cat# 124241; RRID: AB_2800595
Anti-mouse CD28 Pe-Cy7 (clone E18)	Biolegend	Cat# 122014; RRID: AB_604079
Anti-mouse CD4 APC/Fire 810 (clone GK1.5)	Biolegend	Cat# 100479; RRID: AB_2860583
Anti-mouse CD43 PE-Cy5 (clone 1B11)	Biolegend	Cat# 121216; RRID: AB_528811
Anti-mouse CD43 PE-Cy7 (clone 1B11)	Biolegend	Cat# 121218; RRID: AB_528813
Anti-mouse CD44 APC/Fire 750 (clone IM7)	Biolegend	Cat# 103062; RRID: AB_2616727
Anti-mouse CD44 BV421 (clone IM7)	Biolegend	Cat# 103039; RRID: AB_10895752
Anti-mouse CD45.1 AF488 (clone	Biolegend	Cat# 110718; RRID: AB_492862
Anti-mouse CD45.1 APC (clone A20)	Biolegend	Cat# 110714; RRID: AB_313503
Anti-mouse CD45.2 SB550 (clone 104)	Biolegend	Cat# 109861; RRID: AB_2860625
Anti-mouse CD62L BV480 (clone MEL-14)	BD Biosciences	Cat# 746726; RRID: AB_2743990
Anti-mouse CD62L BV510 (clone MEL-14)	Biolegend	Cat# 104441; RRID: AB_2561537
Anti-mouse CD8α BV570 (clone 53-6.7)	Biolegend	Cat# 100740; RRID: AB_2563055
Anti-mouse CD8α BV650 (clone 53-6.7)	Biolegend	Cat# 100742; RRID: AB_2563056
Anti-mouse CD8α BV785 (clone 53-6.7)	Biolegend	Cat# 100750; RRID: AB_2562610
Anti-mouse CXCR3 BV421 (clone CXCR3-173)	Biolegend	Cat# 126521; RRID: AB_10900974
Anti-mouse F4/80 AF488 (clone BM8)	Biolegend	Cat# 123119; RRID: AB_893491
Anti-mouse F4/80 AF647 (clone BM8)	Biolegend	Cat# 123122; RRID: AB_893480
Anti-mouse Granzyme B Pacific Blue (clone GB11)	Biolegend	Cat# 515407; RRID: AB_2562195
Anti-mouse Granzyme B PE (clone NGZB)	Thermofisher	Cat# 12-98898-82; RRID: AB_10870787
Anti-mouse ICOS BV510 (clone C398.4A)	Biolegend	Cat# 313525; RRID: AB_2562642
Anti-mouse ICOS Pe-Cy7 (clone 7E.17G9)	Biolegend	Cat# 117421; RRID: AB_2860636
Anti-mouse IFN-γ AF488 (clone XMG1.2)	Biolegend	Cat# 505815; RRID: AB_493313
Anti-mouse Ki-67 AF488 (clone SolA15)	Thermofisher	Cat# 53-5698-82; RRID: AB_2802330
Anti-mouse KLRG-1 BV711 (clone 2F1/KLRG1)	Biolegend	Cat# 138427; RRID: AB_2629721
Anti-mouse NK1.1 AF488 (clone PK136)	Biolegend	Cat# 108717; RRID: AB_493184
Anti-mouse NK1.1 AF647 (clone PK136)	Biolegend	Cat# 108720; RRID: AB_2132713
Anti-mouse T-BET PE-eFluor610 (clone 4B10)	Biolegend	Cat# 644827; RRID: AB_2565676
Anti-mouse Thy1.1 (clone OX-7)	Biolegend	Cat# 202526; RRID: AB_159547
Anti-mouse TNF-α BV650 (clone MP6-XT22)	Biolegend	Cat# 506333; RRID: AB_2562450
Anti-mouse Vα2 AF488 (clone B20.1)	Biolegend	Cat# 127819; RRID: AB_2687229
CTLA-4 Ig	BioXCell	Cat# BE0099; RRID: AB_10949064
Anti-ICOS	BioXCell	Cat# BE0059; RRID: AB_1107622

REAGENT or RESOURCE	SOURCE	IDENTIFIER
Chemicals, peptides, and recombinant proteins		
α-KGDH$_{932-940}$ (QL9) peptide, QLSPFPFDL	GenScript	N/A
α-KGDH$_{933-941}$ (LL9) peptide, LSPFPFDLL	GenScript	N/A
Murine Leukemia Virus gp70$_{423-431}$ (MuLV) peptide, SPSYVYHQF	GenScript	N/A
Chicken Ovalbumin$_{257-264}$ (OVA) peptide, SIINFEKL	GenScript	N/A
H-2L(d)/QL9 biotinylated monomer	NIH Tetramer Core	N/A
H-2L(d)/LL9 biotinylated monomer	NIH Tetramer Core	N/A
H-2L(d)/MuLV biotinylated monomer	NIH Tetramer Core	N/A
H-2K(b)/OVA biotinylated monomer	NIH Tetramer Core	N/A
H-2D(b)/LCMV gp33 biotinylated monomer	NIH Tetramer Core	N/A
Streptavidin-RPE	Agilent	Cat# PJRS25-1
Streptavidin-APC	Agilent	Cat# PJ27S-1
Mouse IL-15 carrier free	Biolegend	Cat# 566301
Mouse IL-12 carrier free	Biolegend	Cat# 577002
Mouse IFN-γ carrier free	Biolegend	Cat# 575302
Mouse IFN-α carrier free	Biolegend	Cat# 575802
Class B CpG oligonucleotide ODN 1826	Invivogen	Cat# tlrl-1826
DNase lyophilized powder	Worthington Biochemical	Cat# LS0023139
Collagenase type 2	Worthington Biochemical	Cat# LS004176
Critical commercial assays		
CellTrace Violet Cell Proliferation Kit, for flow cytometry	Invitrogen	Cat# C34557
Zombie NIR Fixable Viability Kit	Biolegend	Cat# 423106
Foxp3/Transcription Factor Staining Buffer Set	Invitrogen	Cat# 00-5523-00
Qiashredder columns	Qiagen	Cat# 79654
RNeasy Plus Mini Kit	Qiagen	Cat# 74134
RNAprotect Tissue Reagent	Qiagen	Cat# 76104
1X RBC Lysis Buffer	eBiosciences	Cat# 00-4333-57
SuperScript IV First-Strand Synthesis System kit for reverse transcription	ThermoFisher	Cat# 18091050
ZR-96 DNA Clean and Concentrator kit	Zymo	Cat# D4023
KAPA2G Fast Multiplex Kit for PCR	Roche	Cat# 07961430001
Herculase Fusion DNA Polymerase kit for PCR	Agilent	Cat# 600677
QIAquick PCR Purification Kit	Qiagen	Cat# 28104
Deposited data		
Mouse *TCRB* sequencing results	Johns Hopkins Research Data Repository	Johns Hopkins Data Research Repository: https://doi.org/10.7281/T1/F1GCSB
Experimental models: Organisms/strains		

REAGENT or RESOURCE	SOURCE	IDENTIFIER
Mouse: C57BL/6J	Jackson	Stock# 000664
Mouse: C57BL/6J Ly5.2-Cr (CD45.1)	Jackson	Stock# 003831
Mouse: Balb/cJ	Jackson	Stock# 000651
Mouse: C57Bl/6-Tg(TcraTcrb)1100Mjb/J (OT-I)	Jackson	Stock# 003831
Mouse: B6.129S7-Rag1tm1mom/J (RAG1 knockout)	Jackson	Stock# 002216
Mouse: C3H/HeJ	Jackson	Stock# 000659
Oligonucleotides		
FR3AK-seq *Mus musculus* TCRB PCR primers	Montagne et al.	N/A
Software and algorithms		
FlowJo v10	FlowJo, LLC	https://www.flowjo.com
Prism 9	GraphPad Software	https:www.graphpad.com
SpecroFlo	Cytek	https://cytekbio.com/pages/spectro-flo
R 4.1.1	R Core Team	https://www.R-project.org/; RRID:SCR_001905
RStudio	RStudio Team	http://www.rstudio.org; RRID:SCR_001905
CytoML 2.40	Finak et al.	https://github.com/RGLab/CytoML
flowWorkspace 4.4.0	Finak et al.	https://bioconductor.org/packages/flowWorkspace/; RRID:SCR_001155
flowCore 2.4.0	Hahne et al.	https://bioconductor.org/packages/flowCore/; RRID:SCR_002205
tidyverse	Wickham et al.	https://www.tidyverse.org/; RRID:SCR_019186
CATALYST 1.16.2	Crowell et al.	https://github.com/HelenaLC/CATALYST; RRID:SCR_017127
FlowSOM 2.0.0	Van Gassen et al.	https://bioconductor.org/packages/FlowSOM/; RRID:SCR_016899
ConsensusClusterPlus 1.56.0	Wilkerson and Hayes	https://bioconductor.org/packages/ConsensusClusterPlus/; RRID:SCR_016954
Scater 1.20.1	McCarthy et al.	http://bioconductor.org/packages/scater/; RRID:SCR_015954
ggplot2 3.3.5	Hadley Wickham	https://ggplot2.tidyverse.org/; RRID:SCR_014601
ComplexHeatmap 2.8.0	Gu et al.	https://github.com/jokergoo/ComplexHeatmap; RRID:SCR_017270
Immunarch 0.6.7	Nazarov et al.	https://immunarch.com/; RRID:SCR_023089
Python 3.8.12	Python Software Foundation	https://www.python.org/; RRID:SCR_008394
tcrdist3 0.2.2	Mayer-Blackwell et al.	https://github.com/kmayerb/tcrdist3
pandas 1.3.4	The pandas Development Team	https://pandas.pydata.org/; RRID:SCR_018214
tcrsampler 0.1.9	Mayer-Blackwell et al.	https://github.com/kmayerb/tcrsampler
olga 1.2.4	Sethna et al.	https://github.com/statbiophys/OLGA
ggridges	Claus Wilke	https://wilkelab.org/ggridges

REAGENT or RESOURCE	SOURCE	IDENTIFIER
MiXCR	Bolotin et al.	https://mixcr.com/mixcr/getting-started/installation/
Other		
Anti-APC Microbeads	Miltenyi Biotec	Cat# 130-090-855
Anti-PE Microbeads	Miltenyi Biotec	Cat# 130-048-801
LS magnetic columns	Miltenyi Biotec	Cat# 130-042-401
gentleMACS M Tubes	Miltenyi Biotec	Cat# 130-093-236
CountBright Absolute Counting Beads	ThermoFisher Scientific	Cat# C36950